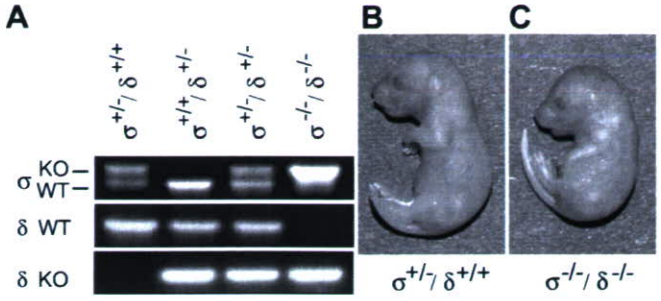

Figure 1. Targeted disruption of the RPTP-σ and RPTP-δ genes. ***A***, PCR-amplified DNA bands using RPTP-σ and RPTP-δ allele-specific primers are shown. In RPTP-σ allele, the amplified knock-out (KO) and wild-type (WT) allele-specific DNA bands are indicated. ***B***, ***C***, E18.5 RPTP-σ/δ double mutants exhibit ptotic postures such as hunchback and wrist drop (***C***), which are not exhibited by non-double-mutant control littermates (***B***) after cesarean section.

Table 1. Offspring of RPTP-σ and RPTP-δ mutant mice derived from parental animals heterozygous for both mutations

		Observed ratio (%)		
Genotype (σ · δ)	Predicted ratio (%)	E18	P0	4 Weeks
+/+ · +/+	6.25	6.85	9.68	7.53
+/− · +/+	12.50	10.96	19.35	25.09
−/− · +/+	6.25	4.11	5.53	3.58
+/+ · +/−	12.50	12.33	8.29	17.20
+/− · +/−	25.00	32.88	21.20	35.84
−/− · +/−	12.50	9.59	15.67	2.87
+/+ · −/−	6.25	9.59	24.29	6.45
+/− · −/−	12.50	8.22	9.22	1.43
−/− · −/−	6.25	5.48	3.23[a]	0.00
		(n = 73)	(n = 217)	(n = 279)

[a]Ratio includes animals found dead at birth.

postnatal day 0 (P0) (n = 217) (Table 1). Furthermore, RPTP-$\sigma^{-/-}/\delta^{+/-}$ and RPTP$\sigma^{+/-}/\delta^{-/-}$ mice had slightly higher mortality rates compared with either single mutant. Within 4 d of birth, 55% of RPTP-$\sigma^{-/-}/\delta^{+/-}$ (n = 18) and 71% of RPTP-$\sigma^{+/-}/\delta^{-/-}$ (n = 14) pups died, whereas 44.4% of RPTP-$\sigma^{-/-}/\delta^{+/+}$ (n = 18) and 14.3% of RPTP-$\sigma^{+/+}/\delta^{-/-}$ (n = 21) died in the same period. Mice heterozygous for either gene had mortality rates not significantly different from wild-type littermates (RPTP-$\sigma^{+/+}/\delta^{+/+}$, 8.7%; RPTP-$\sigma^{+/-}/\delta^{+/+}$, 13.6%; RPTP-$\sigma^{+/+}/\delta^{+/-}$, 5.9%). These findings suggest that RPTP-σ and RPTP-δ exhibit some functional complementarity during development.

To investigate whether RPTP-σ/δ double-mutant mice died before or after birth, cesarean sections were performed at E18.5. Approximately one-sixteenth (5.48%; n = 73) were RPTP-σ/δ double mutant, slightly less than the expected Mendelian ratio, indicating that the RPTP-σ/δ double mutants are viable to late embryogenesis. While, non-double-mutant E18.5 littermates begin to breathe immediately after cesarean section, RPTP-σ/δ double-mutant embryos were never observed to take a breath and died shortly after cesarean section. Furthermore, RPTP-σ/δ double mutants were never observed to move and display kyphosis (hunchback) and carpoptosis (wrist drop) with 100% penetrance (n = 12) as shown in Figure 1*C*. Histological analysis revealed that the alveoli of E18.5 RPTP-σ/δ double-mutant mice (n = 3) were tightly compressed (Fig. 2*C*), consistent with their inability to breathe. We conclude that RPTPσ/δ double mutants die immediately after birth and that death is likely attributable to respiratory failure.

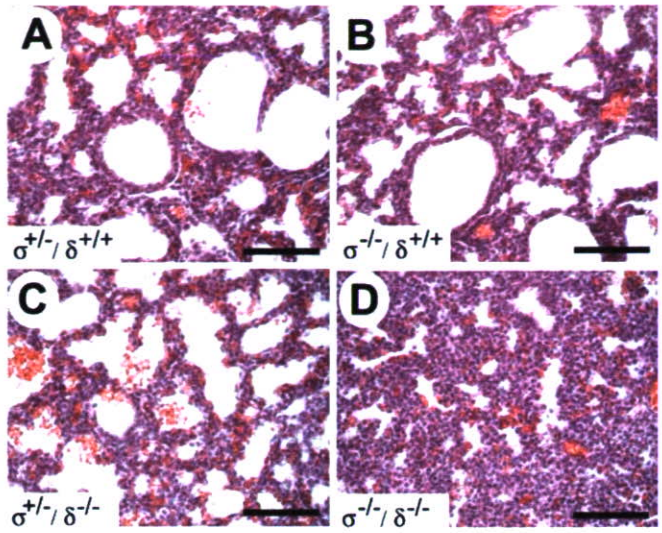

Figure 2. Histological analyses of the lung. ***A–D***, Histology of H&E-stained lung sections prepared from E18.5 embryos 30 min after cesarean section. The alveoli of RPTP-σ/δ double mutants were tightly compressed (***D***), and incompletely extended alveoli were seen in RPTP-$\sigma^{+/-}/\delta^{-/-}$ lung (***C***), compared with RPTP-$\sigma^{+/-}/\delta^{+/+}$ (***A***) and RPTP-$\sigma^{-/-}/\delta^{+/+}$ (***B***) littermates. Scale bars, 50 μm.

Histological analysis of skin, adipose tissue and skeletal muscle

To examine the effects of the mutations on tissue structure, an extensive histological survey was performed. The skin of RPTP-σ/δ double-mutant embryos was abnormal with a semitransparent appearance that was obvious from E15. Although the thickness of the epidermis was not altered in RPTP-σ/δ double mutants (controls, 42 ± 8 μm, n = 18; RPTP-σ/δ double mutants, 43 ± 9 μm, n = 18), the dermis of RPTP-σ/δ double mutants was thinner (control, 109 ± 21 μm, n = 18; RPTP-σ/δ double mutants, 83 ± 14 μm, n = 18; $p < 0.001$) and hair follicles were not fully developed at E18.5 in comparison with control non-double-mutant littermates (Fig. 3*A–D*). Subcutaneous tissues were enlarged, and the compartmentalization of brown adipose tissue was less obvious in RPTP-σ/δ double mutants (Fig. 3*E*,*G*, indicated by **). Furthermore, immunohistochemical analyses using anti-myosin heavy chain antibodies revealed a reduction in the mass of dorsal axial skeletal muscles and limb muscles (Fig. 3*E–J*). In E18.5 RPTP-σ/δ double-mutant embryos, we observed that skeletal muscle fibers were smaller in diameter, with their nuclei centrally localized along the fiber, suggesting the muscles remained immature with their development halted at an early stage of myotube formation (Fig. 3*K*,*L*). These phenotypes, revealed using histological and immunohistochemical staining, were identical in each of the three E18.5 RPTP-σ/δ double-mutant samples analyzed. Although only two E16.5 embryos were analyzed for each genotype, the mean thickness of the diaphragm of these RPTP-σ/δ double-mutant mice was thinner compared with those of wild-type littermates (RPTP-$\sigma^{+/+}/\delta^{+/+}$, 197 ± 15 μm, n = 27; RPTP-σ/δ double mutants, 110 ± 17 μm, n = 27; $p < 0.001$) (Fig. 3*M–P*). Together, these results suggest that the respiratory insufficiency in the double mutants was attributable to skeletal muscle defects, likely caused by the absence of motoneuron innervation, as described below.

Histological differences were not detected in H&E-stained E18.5 heart, liver, kidney, colon, thymus, or spleen of RPTP-σ/δ double mutants (data not shown). In addition, sagittal sections of E18.5 brain were also examined by H&E stain. Although RPTP-σ

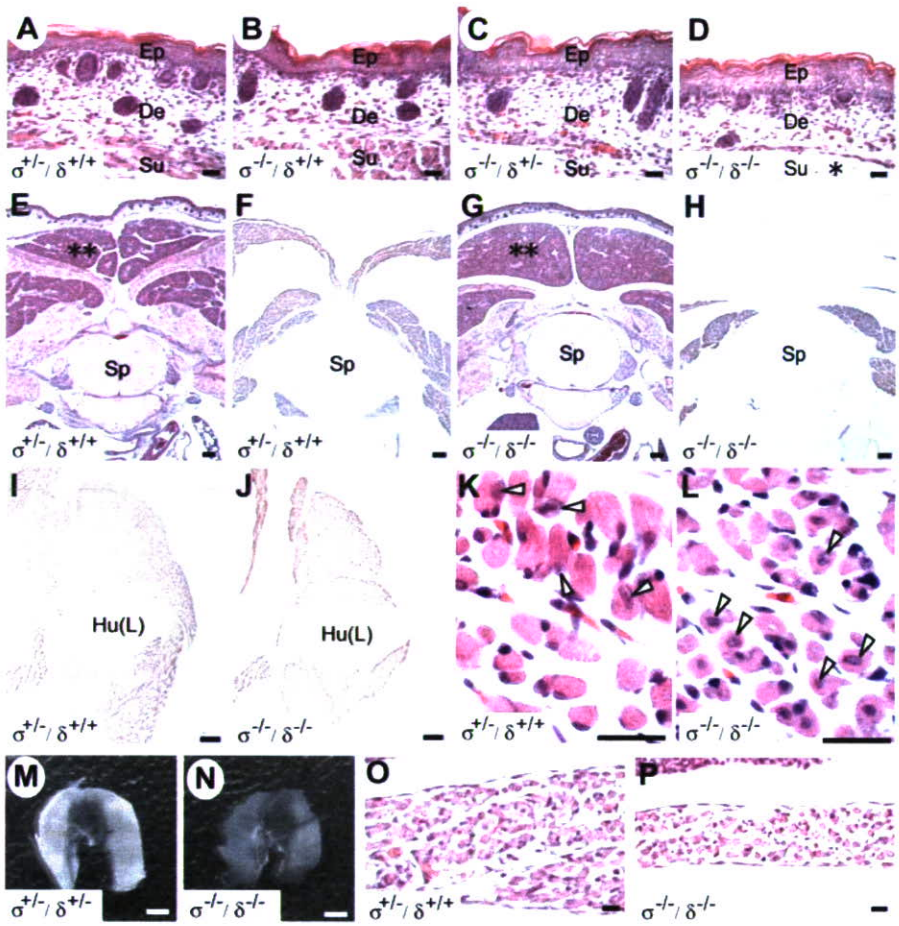

Figure 3. RPTP-σ/δ double-mutant embryos exhibit abnormal muscle development. Comparable transverse sections of E18.5 embryos at forelimb level (***A–L***) and sagittal sections of E16 embryos (***O***, ***P***) were stained with H&E (***A–D***, ***E***, ***G***, ***K***, ***L***, ***O***, ***P***), and skeletal muscles were immunohistochemically visualized with anti-myosin heavy chain antibodies (***F***, ***H***, ***I***, ***J***). ***A–D*** illustrate skin from the embryos' backs. In the RPTP-σ/δ double mutant (***D***), the dermis was thinner than in non-double-mutant littermates (***A–C***), and immature hair follicles were distributed under the epidermis. Subcutaneous tissue was enlarged dropsically in RPTP-σ/δ double mutants (***D***; indicated by *). ***E–H***, Dorsal axial skeletal muscle mass was markedly reduced, and the conformation of brown adipose tissue was not well organized in RPTP-σ/δ double mutants (***G***, ***H***) compared with non-double-mutant littermates (***E***, ***F***) (brown adipose tissues are indicated by **). ***I***, ***J***, Forelimb skeletal muscle mass was also relatively smaller in size in RPTP-σ/δ double mutants (***J***) than in control littermates (***I***). ***K***, ***L***, High magnification of forelimb skeletal muscle. Muscle nuclei are indicated by white arrowheads. In RPTP-σ/δ double mutants, muscle fibers with central nuclei were observed in greater abundance, and the muscle fibers were smaller than those of the non-double-mutant littermates (***K***). ***M–P*** illustrate the diaphragm dissected from a control littermate (***M***) and a RPTP-σ/δ double mutant (***N***) at E18.5. Cross sections of the diaphragm of an E16 RPTP-σ/δ double-mutant (***P***) and a non-double-mutant littermate (***O***), revealed a thinner diaphragm in the RPTP-σ/δ double mutant. Scale bars: ***A–D***, ***K***, ***L***, ***O***, ***P***, 10 μm; ***E–J***, 100 μm; ***M***, ***N***, 1 mm. Ep, Epidermis; De, dermis; Su, subcutaneous tissue; Sp, spinal cord; Hu(L), left humerus.

and RPTP-δ are highly expressed in the developing brain, the gross anatomy of the brain including olfactory bulb, forebrain, hippocampus, cortex, and cerebellum appeared normal in RPTP-σ/δ double mutants (data not shown).

Loss of spinal motoneurons in RPTP-σ/δ double mutants

RPTP-σ/δ double-mutant embryos did not move after cesarean section and appeared paralyzed (Fig. 1*C*). This phenotype is often associated with motoneuron defects, including aberrant neuromuscular junction formation (Misgeld et al., 2002; Brandon et al., 2003). RPTP-σ and RPTP-δ are both highly expressed by spinal motoneurons during embryogenesis (Sommer et al., 1997; Schaapveld et al., 1998). To explore the possibility that motoneuron development may be disrupted by loss of RPTP-σ and RPTP-δ function, transverse sections of spinal cords were examined by Nissl stain (Fig. 4). At E18.5, motoneurons were readily identified by their large cell bodies, large nucleolus, and enriched cellular Nissl bodies in the spinal cords of wild-type embryos (Fig. 4*C*).

In contrast, only a few morphologically abnormal motoneurons, exhibiting smaller cytoplasm with Nissl bodies and an indistinct nucleolus, were found in E18.5 RPTP-σ/δ double mutants (Fig. 4*D*, arrows). No obvious abnormalities were observed in the dorsal root ganglia (DRGs) (Fig. 4*E*,*F*) or sympathetic ganglia (SGs) (Fig. 4*G*,*H*). Expression of the motoneuron-specific markers, Islet-1/2 and ChAT (Tsuchida et al., 1994; Pfaff et al., 1996; Helmbacher et al., 2000), was then examined on transverse sections of E13 and E18.5 spinal cords at the level of the third (C3) and fifth (C5) cervical vertebrae, respectively (Fig. 5*A–D*). Although the number of Islet-1/2-immunopositive motoneurons per hemiventral motor column appeared normal in RPTP-σ/δ double mutants at E13 (Fig. 5*E*), the number of ChAT-immunopositive motoneurons detected in RPTP-σ/δ double mutants at E18.5 was significantly reduced (Fig. 5*F*, $^{**}p < 0.0001$). These findings identify a major motoneuron deficit in RPTP-σ/δ double mutants that occurs late in embryogenesis between E13 and E18.5, during motoneuron axon extension. Additionally, a smaller but significant decrease in the number of ChAT-immunopositive motoneurons was also detected in RPTP-$\sigma^{-/-}$/$\delta^{+/-}$ embryos compared with wild-type or embryos mutant for either RPTP-σ or RPTP-δ alone (Fig. 5*F*, $^{*}p < 0.001$). That a single gene dose of RPTP-σ is sufficient for levels of motoneuron survival in RPTP-$\sigma^{+/-}$/$\delta^{-/-}$ that are not different from control, suggests that RPTP-σ may make a larger essential contribution to motoneuron survival than does RPTP-δ.

Altered innervation of the diaphragm by the phrenic nerve in RPTP-σ/δ double mutants

Motoneurons depend on target-derived trophic support to survive. During late embryogenesis, cell death matches the number of motoneurons with the size of the muscle targets being innervated (Banks and Noakes, 2002). We hypothesized that defects in the ability of motoneurons to reach and innervate muscle targets might contribute to the motoneuron loss detected in RPTP-σ/δ double mutants (Figs. 4, 5). To test this, we examined the projection of the phrenic nerve at various developmental stages using whole-mount immunochemistry and a neurofilament (NF) antibody (2H3). The phrenic nerve contains motor axons that originate in the spinal cord between C3 and C5 and extend to the diaphragm. It then forms three characteristic branches on the surface of the diaphragm: two sternocostal branches and one

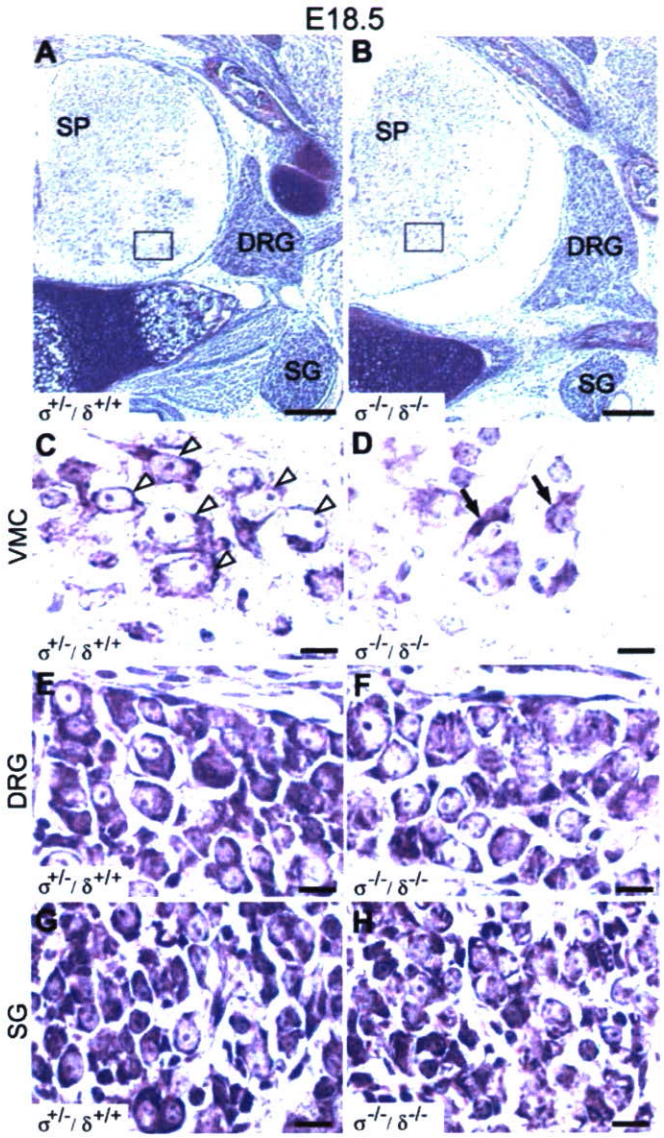

Figure 4. RPTP-σ/δ double mutants exhibit major defects in motoneurons but not DRG or SG neurons. ***A***, ***B***, Nissl-stained spinal cord, DRG, and SG at the forelimb level are shown. ***C***, ***D***, High-magnification views of ventral horn motor columns from the regions framed in ***A*** and ***B***, respectively. Multiple motoneurons containing a large nucleolus are readily visible in the non-double-mutant littermate (***C***, arrowheads). In contrast, RPTP-σ/δ double mutants contained reduced numbers of large motoneurons and degenerating motoneurons in the ventral horn of the spinal cord (***D***, arrows) compared with non-double-mutant littermates (***C***). ***E*** and ***F***, and ***G*** and ***H*** illustrate high-magnification views of DRG and SG, respectively. Morphologically, there were no significant differences in DRG and SG between each genotype. Scale bars: ***A***, ***B***, 100 μm; ***C–H***, 10 μm. SP, Spinal cord; VMC, ventral motor column.

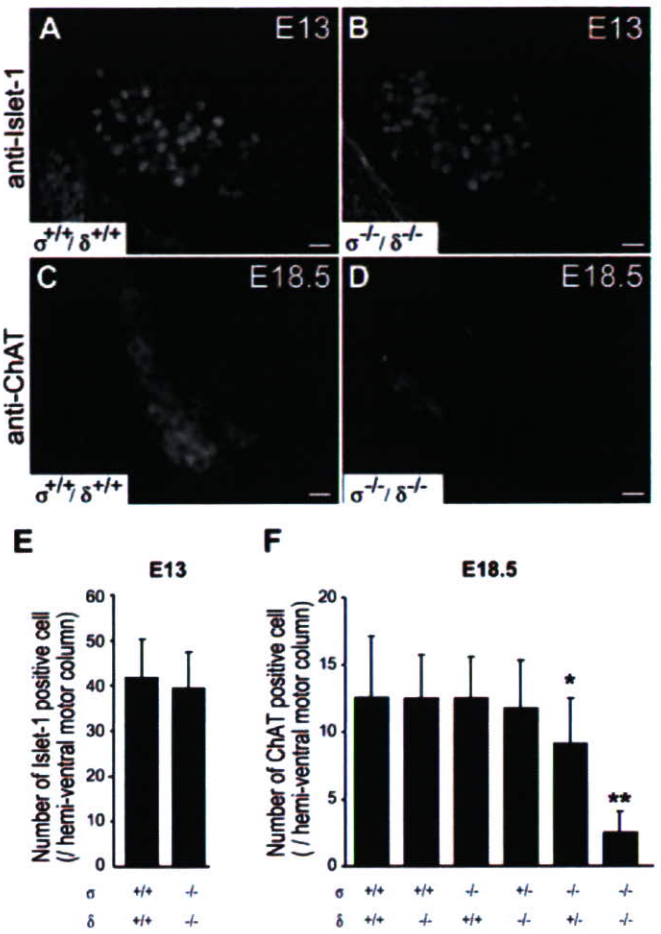

Figure 5. Loss of spinal motoneurons in RPTP-σ/δ double mutants. ***A–D***, Islet-1/2 and ChAT immunofluorescence identifies ventral motoneurons in spinal cords (C3–C5) at E13 (***A***, ***B***) and E18.5 (***C***, ***D***), respectively. At E13, similar populations of Islet-1/2-immunopositive motoneurons were detected in both wild-type and RPTP-σ/δ double mutants (***A***, ***B***). ***E***, The number of Islet-1/2-immunopositive cells showed no significant difference ($p = 0.223$). At E18, ChAT-immunopositive motoneurons were seldom detected in E18.5 RPTP-σ/δ double mutants (***C***, ***D***). ***F***, Quantitative analysis revealed that numbers of ChAT-immunopositive cells were significantly decreased in RPTP-$\sigma^{-/-}/\delta^{+/-}$ (*$p < 0.001$) and RPTP-σ/δ double mutants (**$p < 0.0001$). Error bars indicate SD. Scale bars: ***A–D***, 10 μm.

crural branch (a schematic is included in the supplemental material, available at www.jneurosci.org). In E10.5 RPTP-σ/δ double mutants, the phrenic nerve descends normally from the spinal cord (data not shown) and reaches the diaphragm at E12 ($n = 3$) (Fig. 6*A*). However, in E13.5 RPTP-σ/δ double-mutant embryos, the phrenic motor axons extend aberrantly on the surface of the diaphragm (Fig. 6*E*,*F*) ($n = 2$). Although the phrenic nerve appears to reach the appropriate initial location on the diaphragm, the two main sternocostal branches that normally defasciculate from the main nerve appear to have retracted (Fig. 6*F*, arrowhead), and only a tiny residual projection extends toward the crus (Fig. 6*E*,*F*, white arrowheads). These phrenic nerve abnormalities were identical in the two individual E13.5 RPTP-σ/δ double mutants examined. Furthermore, analyses of E15.5 ($n = 2$) and E18.5 ($n = 3$) double mutants revealed the complete absence of sternocostal branches on the diaphragm (E15.5) (Fig. 7*E*,*F*) (E18.5) (data not shown). Each of the total of seven RPTP-σ/δ double mutants analyzed (E13.5, E15.5, and E18.5) exhibited aberrant phrenic nerve phenotypes, consistent with the conclusion that these phrenic nerve defects are 100% penetrant in the absence of RPTP-σ/δ function. At E13.5 and E15.5, the capillaceous nerves normally defasciculate from the major sternocostal branches (Figs. 6*C*, 7*A*,*B*); however, capillaceous nerves were seldom observed in either the RPTP-$\sigma^{-/-}/\delta^{+/-}$ (data not shown) or RPTP-$\sigma^{+/-}/\delta^{-/-}$ genotypes (Figs. 6*D*, 7*C*,*D*). In contrast, the innervation of the diaphragm in RPTP-σ and RPTP-δ single-mutant littermates appeared normal (Fig. 7*G*,*H*). To further substantiate these observations, we performed quantitative analysis on anti-NF-stained diaphragms at E15.5 by counting each nerve branch point. As shown in Figure 7*I*, the total number of branch points was decreased in RPTP-$\sigma^{+/-}/\delta^{-/-}$ ($n = 3$) and RPTP-$\sigma^{-/-}/\delta^{+/-}$ ($n = 2$) embryos compared with non-double mutants, including the RPTP-σ ($n = 3$) and RPTP-δ ($n = 2$) single mutants.

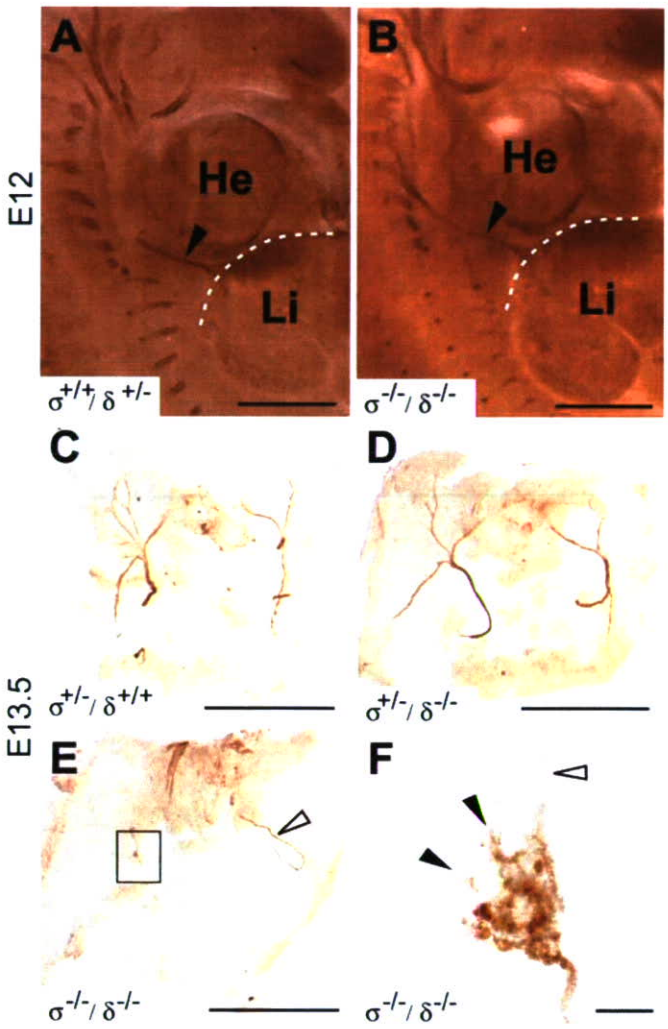

Figure 6. Aberrant innervation of the diaphragm in RPTP-σ/δ double mutants. Tissues were immunohistochemically labeled with anti-neurofilament antibodies (2H3). ***A***, ***B***, Sagittal views of non-double-mutant littermates RPTP-$\sigma^{+/+}/\delta^{+/-}$ (***A***) and RPTP-$\sigma^{-/-}/\delta^{-/-}$ (***B***) at E12 are shown. Dotted lines indicate the diaphragm. Phrenic nerves (arrowheads) extended from cervical spinal cord and onto the diaphragm normally in the RPTP-σ/δ double mutant at E12 (***B***) ($n = 3$). ***C–F***, By E13.5, phrenic nerves branched out into three major nerves on the diaphragm of control RPTP-$\sigma^{+/-}/\delta^{+/+}$ (***C***); however, only one tiny nerve was seen to extend onto the diaphragm of RPTP-$\sigma^{-/-}/\delta^{-/-}$ (***E***) ($n = 2$). The number of capillaceous nerves found to defasciculate from the major nerve trunk onto the diaphragm was slightly less in E13.5 RPTP-$\sigma^{+/-}/\delta^{-/-}$ mice (***D***) ($n = 1$). ***F***, High-magnification view of the frame in ***E***. Retracting sternocostal nerves are indicated by black arrowheads. Crural nerves are indicated by white arrowheads. Scale bars, 1 mm. He, Heart; Li, liver.

Comparison of these findings with Figure 5*F* indicates that the defect in branching is more sensitive to RPTP loss of function than is motoneuron survival: E18.5 RPTP-$\sigma^{+/-}/\delta^{-/-}$ exhibit no significant difference in motoneuron number compared with control, whereas E18.5 RPTP-$\sigma^{-/-}/\delta^{+/-}$ exhibit a modest, albeit significant, reduction of the number of motoneurons, ~70% of control (Fig. 5*F*). In contrast, E18.5 double knock-out RPTP-$\sigma^{-/-}/\delta^{-/-}$ exhibit severely reduced numbers of motoneurons, ~20% of control, and no branching from the sternocostal phrenic nerve. Although these findings suggest a relationship between innervation and survival, we have not ruled out the possibility that these two phenotypes may be dissociable. The intermediate nerve branch phenotype found in RPTP-$\sigma^{-/-}/\delta^{+/-}$ and RPTP-$\sigma^{+/-}/\delta^{-/-}$ embryos provides evidence that RPTP-σ and RPTP-δ have at least partially redundant functions and normally make an additive contribution to the branching of phrenic projections. We conclude that RPTP-σ and RPTP-δ make an essential functional contribution to normal muscle innervation by motoneurons. Table 2 provides a summary of the quantitative analyses of the various phenotypes described.

Discussion

Here, we demonstrate that RPTP-σ and RPTP-δ make a complementary contribution to motoneuron axon targeting during mammalian development. In the absence of either RPTP-σ or RPTP-δ, mice exhibit severe growth retardation, increased postnatal lethality, and motor dysfunction (Elchebly et al., 1999; Wallace et al., 1999; Uetani et al., 2000). Unlike in invertebrates, in which it has been shown that LAR-RPTP loss of function causes defects in axon extension by motoneurons (Desai et al., 1996, 1997; Krueger et al., 1996), photoreceptors (Garrity et al., 1999; Newsome et al., 2000), and commissural neurons (Sun et al., 2000), mutation of RPTP-σ or RPTP-δ has not been found to generate gross defects in axon guidance in mammals. Among the three members of the mammalian LAR-RPTP subfamily, LAR is most broadly expressed and, in particular, is expressed in many non-neural tissues. In contrast, RPTP-σ and RPTP-δ are both expressed in the CNS during neural development, often by the same cell types (Yan et al., 1993; Mizuno et al., 1994; Sommer et al., 1997; Schaapveld et al., 1998). We postulated that RPTP-σ and RPTP-δ likely play important roles during neural development but that they may compensate for each other functionally in single RPTP mutant mice. To test this hypothesis, we generated mice lacking both RPTP-σ and RPTP-δ. Here, we report that RPTP-σ/δ double-mutant mice exhibit a dramatic neuromuscular phenotype, with complete absence of movement, absence of breathing, and death shortly after birth. Histological analysis confirmed that the lungs fail to inflate in the double mutants (Fig. 2), likely because of inadequate innervation of the diaphragm (Figs. 6, 7). Notably, both RPTP-$\sigma^{-/-}/\delta^{+/-}$ and RPTP$\sigma^{+/-}/\delta^{-/-}$ mice exhibit reduced average life spans compared with either single mutant, suggesting some complementary function. RPTP-σ/δ double mutants also exhibited histological defects in the dermis, brown adipose tissue, and skeletal muscle (Fig. 3). Aberrant innervation by motoneurons is a likely cause of the skeletal muscle defects found in RPTP-σ/δ double mutants. However, we have not excluded the possibility of other roles for RPTP-σ and RPTP-δ, because both are expressed by mesodermal tissues during embryogenesis (Schaapveld et al., 1998).

Consistent with the complete absence of movement in RPTP-σ/δ double mutants, histological examination of the embryonic spinal cord revealed that the majority of ChAT-immunopositive motoneurons were lost by E18.5 (Fig. 5*D*,*F*). However, at E13, the number of Islet-1/2-immunopositive motoneurons observed in RPTP-σ/δ double mutants was indistinguishable from wild type (Fig. 5*E*), suggesting that motoneuron loss is linked to defects in the late stages of axon extension, rather than altered motoneuron differentiation or development. This hypothesis is supported by our findings that phrenic axons in the double mutant appear to exit the spinal cord normally at E12 and appropriately extend toward the diaphragm (Fig. 6*B*), yet at E13.5, the terminal axonal branches that normally contact the diaphragm are severely stunted in the double mutants (Fig. 6*E*,*F*). By E15.5, the branches are absent (Fig. 7*E*,*F*) and presumably have been retracted. This interpretation is supported by our observation of a similar distribution of residual branches in the two E13.5 RPTP-σ/δ double mutants examined (Fig. 6*F*, black arrowheads). Consistent with retraction of these axons at E15.5, the loss of mo-

toneuron cell bodies was clearly evident by E18.5 (Fig. 5*D*,*F*). These results suggest that spinal motoneurons are lost in the double mutants as a consequence of their inability to establish appropriate contacts with muscle targets.

Our analyses reveal the absence of specific phrenic nerve branches in RPTP-σ/δ double mutants and reduced branching in RPTP-$\sigma^{+/-}/\delta^{-/-}$ and RPTP-$\sigma^{-/-}/\delta^{+/-}$ (Fig. 7*I*). These results suggest that the absence of RPTP-σ and RPTP-δ may suppress the ability of axons to defasciculate from the phrenic nerve. Fasciculation is regulated by the relative affinity of the interactions between neighboring axons, and the affinity between an axon and its immediate environment. Interestingly, axon guidance defects with similarities to what we report here have been observed as a result of RPTP loss-of-function mutations in *Drosophila*. Loss of DLAR function, the *Drosophila* ortholog of both RPTP-σ and RPTP-δ, causes SNb motoneurons to fail to recognize appropriate muscle targets and generates errors in synapse formation (Krueger et al., 1996). Furthermore, mutation of the *Drosophila* RPTPs DPTP99A and DPTP69D results in misdirected motoneuron axon growth, defects in motoneuron axon defasciculation, and causes growth cones to stall as they approach muscle targets (Desai et al., 1996). These RPTP loss-of-function mutations in *Drosophila* produced defects in motoneuron axon guidance similar to those produced by CAM gain of function mutations (Lin and Goodman, 1994; Nose et al., 1994). Moreover, using RNA interference in the chick embryo, Stepanek et al. (2005) provided evidence that dorsal motor nerve fasciculation is disrupted by knock-down of either RPTP-σ or RPTP-δ. Thus, it is tempting to speculate that RPTP-σ and RPTP-δ play a conserved role during mouse neural development, tempering adhesive interactions, thereby allowing motoneurons to appropriately defasciculate, extend, and make synaptic connections.

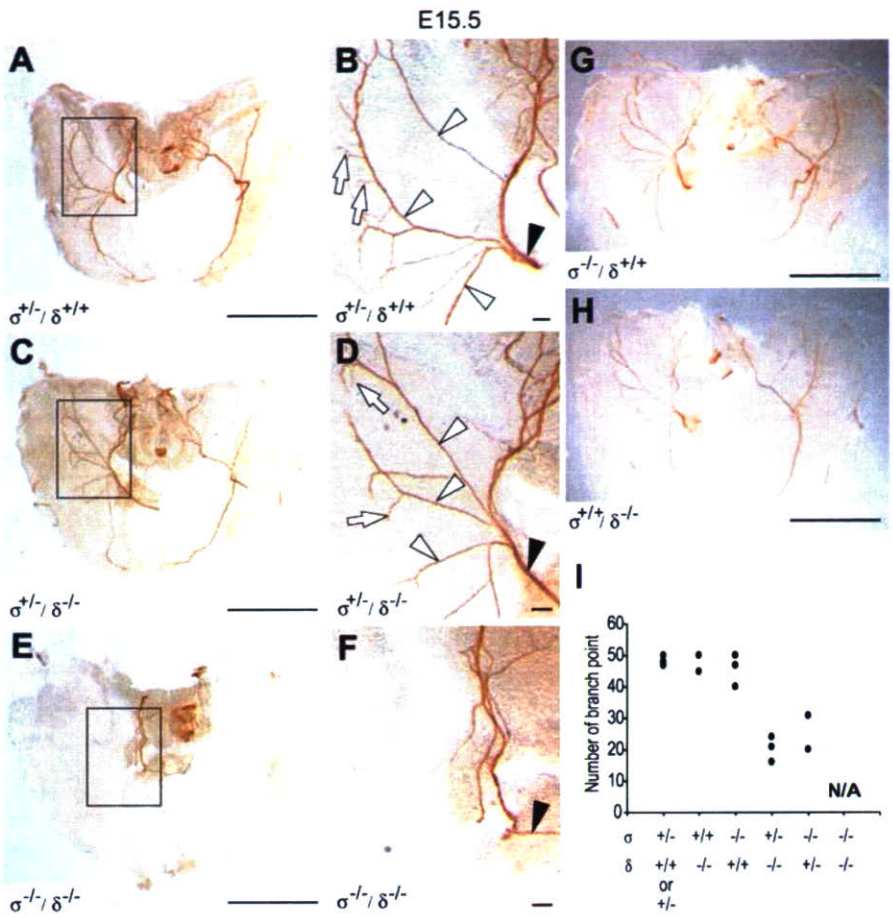

Figure 7. Complete absence of sternocostal nerves in RPTP-σ/δ double mutants at E15.5. Diaphragms stained with anti-neurofilament antibodies (2H3) at E15.5 are shown (***A–H***). ***B***, ***D***, ***F***, High-magnification views of the frames in ***A***, ***C***, and ***E***. In control RPTP-$\sigma^{+/-}/\delta^{+/+}$ mice, phrenic axons extend normally on surface of the diaphragm (***A***), and numerous capillaceous nerves defasciculate from the trunk (***B***). Intramuscular branches and capillaceous nerves are indicated by white arrowheads and white arrows, respectively (***B***, ***C***). Reduced capillaceous nerve branching was observed in RPTP-$\sigma^{+/-}/\delta^{-/-}$ mice (***C***, ***D***). In the RPTP-σ/δ double mutants, the intramuscular branches were absent (***E***, ***F***), and the main nerve was clearly thinner in comparison with the non-double-mutant littermates (***B***, ***D***, ***F***; indicated by arrowhead). The innervation of the diaphragm in RPTP-σ and RPTP-δ single-mutant littermates appeared normal (***G***, ***H***). The number of branch point from the sternocostal phrenic nerve in RPTP-$\sigma^{+/-}/\delta^{+/+\text{ or }+/-}$ ($n = 3$), RPTP-$\sigma^{+/+}/\delta^{-/-}$ ($n = 2$), RPTP-$\sigma^{-/-}/\delta^{+/+}$ ($n = 3$), RPTP-$\sigma^{+/-}/\delta^{-/-}$ ($n = 3$), RPTP-$\sigma^{-/-}/\delta^{+/-}$ ($n = 2$) is illustrated in ***I***. Scale bars: ***A***, ***C***, ***E***, ***G***, ***H***, 1 mm; ***B***, ***D***, ***F***, 100 μm.

Quantitative analyses indicated that RPTP-$\sigma^{+/-}/\delta^{-/-}$ and RPTP-$\sigma^{-/-}/\delta^{+/-}$ mutants exhibited intermediate phenotypes in motoneuron survival and phrenic nerve branching, whereas no significant defect in either of the RPTP-σ or RPTP-δ single mutants was detected (Figs. 5, 7*I*). These results provide strong evidence that RPTP-σ and RPTP-δ complement each other functionally during axon targeting by mammalian motoneurons.

In contrast to the severe motoneuron defects reported, we have not observed abnormal phenotypes in sensory neurons, such as DRG neurons, nor in sympathetic neurons. RPTP-σ is expressed by both motoneurons and sensory neurons. Motoneurons express RPTP-δ but not LAR, whereas the converse is the case for sensory neurons (Sommer et al., 1997; Schaapveld et al., 1998), suggesting that LAR may be able to compensate for the loss of RPTP-σ in sensory neurons in the double mutant. Interestingly, recent findings indicate that RPTP-σ and LAR influence axon regeneration in the adult CNS. The absence of LAR delayed axonal regeneration *in vivo* after injury to the sciatic nerve, a mixed sensory and motor nerve (Xie et al., 2001; Van der Zee et al., 2003). In contrast, in the RPTP-σ mutant mice, axon regeneration in the sciatic, facial, and optic nerves was enhanced after axotomy (McLean et al., 2002; Thompson et al., 2003; Saphieha et al., 2005). These findings imply that, although LAR-RPTPs may sometimes exhibit redundant functions, the expression of different LAR-RPTPs may also have different functional consequences in some neuronal cell types.

Although the ligands and signal transduction mechanisms associated with LAR-RPTPs are not well understood, recent studies have provided evidence that the extracellular domain of cRPTP-σ binds to matrix-associated heparan sulfate proteoglycans (HSPGs) (Haj et al., 1999; Aricescu et al., 2002), cues that influence axon guidance and play multiple essential roles during neural development (Inatani et al., 2003). The cRPTP-σ extracellular domain also binds developing skeletal myotubes, although the putative ligand involved has not been identified (Sajnani-Perez et al., 2003). The extracellular matrix laminin-nidogen complex has also been identified as a ligand for the LAR-FNIII

Table 2. Primary phenotypes in RPTP-σ/δ double mutants

	Paralysis	Diaphragm dystrophy[a]	Aberrant phrenic nerve projection[b]		Decreased number of motoneurons			
	E18.5	E16.5–E18.5	E12	E13.5–E18.5	E13		E18.5	
Genotype (σ · δ)	Pen (%)	Pen (%)	Pen (%)	Pen (%)	Pen[c] (%)	Red (%)	Pen[c] (%)	Red (%)
+/+ · +/+	0 (7)	0 (4)	0 (2)	0 (5)	0 (5)	0 (5)	0 (4)	0 (4)
+/− · +/+	0 (9)	0 (7)	—	0 (4)	—	—	—	—
−/− · +/+	0 (5)	0 (2)	—	0 (7)	—	—	0 (2)	0 (2)
+/+ · +/−	0 (12)	0 (7)	0 (2)	0 (2)	—	—	—	—
+/− · +/−	0 (27)	0 (19)	—	0 (1)	—	—	—	—
−/− · +/−	0 (8)	0 (5)	—	100[d] (4)	—	—	50 (4)	30 (4)
+/+ · −/−	0 (9)	0 (5)	—	0 (6)	—	—	0 (3)	0 (3)
+/− · −/−	0 (10)	0 (7)	—	100[d] (5)	—	—	0 (2)	0 (2)
−/− · −/−	100 (15)	100 (6)	0 (3)	100[e] (7)	0 (3)	0 (3)	100 (4)	85 (4)

The number of animals analyzed is indicated in parentheses. Pen (%), Percentage of penetrance; Red (%), percentage of reduction compared with control animals; —, data are not available.

[a]Scored using histological sections at E16.5 and dissected diaphragms at E18.5.

[b]Scored using whole-mount anti-NF-stained diaphragms.

[c]Scored positive if statistically significant by Student's *t* test ($p < 0.05$) against control animals.

[d]Showing less branching phenotype.

[e]Showing loss of sternocostal (intramuscular) nerves.

domain 5 (FN5) (O'Grady et al., 1998). This domain of LAR is highly conserved in all LAR-RPTPs, implicating laminin-nidogen as a potential ligand for RPTP-σ and RPTP-δ as well. Notably, laminins make numerous contributions to neural development, including influencing nerve–muscle synapse formation (Colognato and Yurchenco, 2000).

The intracellular domains of LAR-RPTPs are reported to interact with α-Liprins (LAR interacting proteins) (Pulido et al., 1995) and β-catenin (Kypta et al., 1996; Muller et al., 1999), and these interactions are implicated in the maintenance of hippocampal excitatory synapses (Dunah et al., 2005). The other known mechanisms of downstream signal transduction regulated by LAR-RPTPs point to a role in the control of actin cytoskeletal organization. For example, the DH-GEF (Dbl-homology guanine nucleotide exchange factor) Trio, a key regulator of the small Rho GTPase, regulates actin dynamics in axon growth cones (Lin and Greenberg, 2000) and is functionally downstream of *Drosophila* DLAR (Bateman et al., 2000). Furthermore, Trio binds Abelson tyrosine kinase (Abl) and Enabled (Ena), both of which are DLAR substrates (Wills et al., 1999). Reducing Trio activity potentiates the motor axon guidance defects produced by DLAR loss of function, which is consistent with Trio collaborating with DLAR during axon guidance (Bateman et al., 2000). Interestingly, mice lacking Trio exhibit phenotypic defects similar to those reported here for RPTP-σ/δ double mutants. These include deficiencies in muscle development (O'Brien et al., 2000), which are consistent with the RPTP-σ/δ double-mutant phenotypes, suggesting that the functional relationship between these genes may be conserved in mammalian neural development. We provide evidence that RPTP-σ and RPTP-δ play functionally complementary roles during murine neural development and together make an essential contribution to appropriate motoneuron targeting. These findings identify a conserved role for the LAR subfamily of RPTPs, regulating motoneuron axon extension in both invertebrates and vertebrates.

References

Aricescu AR, McKinnell IW, Halfter W, Stoker AW (2002) Heparan sulfate proteoglycans are ligands for receptor protein tyrosine phosphatase sigma. Mol Cell Biol 22:1881–1892.

Banks GB, Noakes PG (2002) Elucidating the molecular mechanisms that underlie the target control of motoneuron death. Int J Dev Biol 46:551–558.

Bateman J, Shu H, Van Vactor D (2000) The guanine nucleotide exchange factor trio mediates axonal development in the *Drosophila* embryo. Neuron 26:93–106.

Beltran PJ, Bixby JL (2003) Receptor protein tyrosine phosphatases as mediators of cellular adhesion. Front Biosci 8:d87–d99.

Brady-Kalnay SM, Tonks NK (1995) Protein tyrosine phosphatases as adhesion receptors. Curr Opin Cell Biol 7:650–657.

Brandon EP, Lin W, D'Amour KA, Pizzo DP, Dominguez B, Sugiura Y, Thode S, Ko CP, Thal LJ, Gage FH, Lee KF (2003) Aberrant patterning of neuromuscular synapses in choline acetyltransferase-deficient mice. J Neurosci 23:539–549.

Clandinin TR, Lee CH, Herman T, Lee RC, Yang AY, Ovasapyan S, Zipursky SL (2001) *Drosophila* LAR regulates R1–R6 and R7 target specificity in the visual system. Neuron 32:237–248.

Colognato H, Yurchenco PD (2000) Form and function: the laminin family of heterotrimers. Dev Dyn 218:213–234.

Desai C, Purdy J (2003) The neural receptor protein tyrosine phosphatase DPTP69D is required during periods of axon outgrowth in *Drosophila*. Genetics 164:575–588.

Desai CJ, Popova E, Zinn K (1994) A *Drosophila* receptor tyrosine phosphatase expressed in the embryonic CNS and larval optic lobes is a member of the set of proteins bearing the "HRP" carbohydrate epitope. J Neurosci 14:7272–7283.

Desai CJ, Gindhart Jr JG, Goldstein LS, Zinn K (1996) Receptor tyrosine phosphatases are required for motor axon guidance in the *Drosophila* embryo. Cell 84:599–609.

Desai CJ, Krueger NX, Saito H, Zinn K (1997) Competition and cooperation among receptor tyrosine phosphatases control motoneuron growth cone guidance in *Drosophila*. Development 124:1941–1952.

Dodd J, Morton SB, Karagogeos D, Yamamoto M, Jessell TM (1988) Spatial regulation of axonal glycoprotein expression on subsets of embryonic spinal neurons. Neuron 1:105–116.

Dunah AW, Hueske E, Wyszynski M, Hoogenraad CC, Jaworski J, Pak DT, Simonetta A, Liu G, Sheng M (2005) LAR receptor protein tyrosine phosphatases in the development and maintenance of excitatory synapses. Nat Neurosci 8:458–467.

Elchebly M, Wagner J, Kennedy TE, Lanctot C, Michaliszyn E, Itie A, Drouin J, Tremblay ML (1999) Neuroendocrine dysplasia in mice lacking protein tyrosine phosphatase sigma. Nat Genet 21:330–333.

Garrity PA, Lee CH, Salecker I, Robertson HC, Desai CJ, Zinn K, Zipursky SL (1999) Retinal axon target selection in *Drosophila* is regulated by a receptor protein tyrosine phosphatase. Neuron 22:707–717.

Haj F, McKinnell I, Stoker A (1999) Retinotectal ligands for the receptor tyrosine phosphatase CRYPalpha. Mol Cell Neurosci 14:225–240.

Helmbacher F, Schneider-Maunoury S, Topilko P, Tiret L, Charnay P (2000) Targeting of the EphA4 tyrosine kinase receptor affects dorsal/ventral pathfinding of limb motor axons. Development 127:3313–3324.

Inatani M, Irie F, Plump AS, Tessier-Lavigne M, Yamaguchi Y (2003) Mammalian brain morphogenesis and midline axon guidance require heparan sulfate. Science 302:1044–1046.

Johnson KG, Holt CE (2000) Expression of CRYP-alpha, LAR, PTP-delta, and PTP-rho in the developing *Xenopus* visual system. Mech Dev 92:291–294.

Johnson KG, Van Vactor D (2003) Receptor protein tyrosine phosphatases in nervous system development. Physiol Rev 83:1–24.

Krueger NX, Van Vactor D, Wan HI, Gelbart WM, Goodman CS, Saito H (1996) The transmembrane tyrosine phosphatase DLAR controls motor axon guidance in *Drosophila*. Cell 84:611–622.

Kypta RM, Su H, Reichardt LF (1996) Association between a transmembrane protein tyrosine phosphatase and the cadherin-catenin complex. J Cell Biol 134:1519–1529.

Lin DM, Goodman CS (1994) Ectopic and increased expression of Fasciclin II alters motoneuron growth cone guidance. Neuron 13:507–523.

Lin MZ, Greenberg ME (2000) Orchestral maneuvers in the axon: trio and the control of axon guidance. Cell 101:239–242.

Maurel-Zaffran C, Suzuki T, Gahmon G, Treisman JE, Dickson BJ (2001) Cell-autonomous and -nonautonomous functions of LAR in R7 photoreceptor axon targeting. Neuron 32:225–235.

McLean J, Batt J, Doering LC, Rotin D, Bain JR (2002) Enhanced rate of nerve regeneration and directional errors after sciatic nerve injury in receptor protein tyrosine phosphatase sigma knock-out mice. J Neurosci 22:5481–5491.

Misgeld T, Burgess RW, Lewis RM, Cunningham JM, Lichtman JW, Sanes JR (2002) Roles of neurotransmitter in synapse formation: development of neuromuscular junctions lacking choline acetyltransferase. Neuron 36:635–648.

Mizuno K, Hasegawa K, Ogimoto M, Katagiri T, Yakura H (1994) Developmental regulation of gene expression for the MPTP delta isoforms in the central nervous system and the immune system. FEBS Lett 355:223–228.

Muller T, Choidas A, Reichmann E, Ullrich A (1999) Phosphorylation and free pool of beta-catenin are regulated by tyrosine kinases and tyrosine phosphatases during epithelial cell migration. J Biol Chem 274:10173–10183.

Newsome TP, Asling B, Dickson BJ (2000) Analysis of *Drosophila* photoreceptor axon guidance in eye-specific mosaics. Development 127:851–860.

Nose A, Takeichi M, Goodman CS (1994) Ectopic expression of connectin reveals a repulsive function during growth cone guidance and synapse formation. Neuron 13:525–539.

O'Brien SP, Seipel K, Medley QG, Bronson R, Segal R, Streuli M (2000) Skeletal muscle deformity and neuronal disorder in Trio exchange factor-deficient mouse embryos. Proc Natl Acad Sci USA 97:12074–12078.

O'Grady P, Thai TC, Saito H (1998) The laminin-nidogen complex is a ligand for a specific splice isoform of the transmembrane protein tyrosine phosphatase LAR. J Cell Biol 141:1675–1684.

Pfaff SL, Mendelsohn M, Stewart CL, Edlund T, Jessell TM (1996) Requirement for LIM homeobox gene Isl1 in motor neuron generation reveals a motor neuron-dependent step in interneuron differentiation. Cell 84:309–320.

Pulido R, Serra-Pages C, Tang M, Streuli M (1995) The LAR/PTP delta/PTP sigma subfamily of transmembrane protein-tyrosine-phosphatases: multiple human LAR, PTP delta, and PTP sigma isoforms are expressed in a tissue-specific manner and associate with the LAR-interacting protein LIP. 1. Proc Natl Acad Sci USA 92:11686–11690.

Sajnani-Perez G, Chilton JK, Aricescu AR, Haj F, Stoker AW (2003) Isoform-specific binding of the tyrosine phosphatase PTPsigma to a ligand in developing muscle. Mol Cell Neurosci 22:37–48.

Saphieha PS, Duplan L, Uetani N, Joly S, Tremblay ML, Kennedy TE, Di Polo A (2005) Receptor protein tyrosine phosphatase sigma inhibits axon regrowth in the adult injured CNS. Mol Cell Neurosci 28:625–635.

Schaapveld RQ, Schepens JT, Bachner D, Attema J, Wieringa B, Jap PH, Hendriks WJ (1998) Developmental expression of the cell adhesion molecule-like protein tyrosine phosphatases LAR, RPTPdelta and RPTP-sigma in the mouse. Mech Dev 77:59–62.

Sommer L, Rao M, Anderson DJ (1997) RPTP delta and the novel protein tyrosine phosphatase RPTP psi are expressed in restricted regions of the developing central nervous system. Dev Dyn 208:48–61.

Stepanek L, Stoker AW, Stoeckli E, Bixby JL (2005) Receptor tyrosine phosphatases guide vertebrate motor axons during development. J Neurosci 25:3813–3823.

Stoker AW, Gehrig B, Haj F, Bay BH (1995) Axonal localisation of the CAM-like tyrosine phosphatase CRYP alpha: a signalling molecule of embryonic growth cones. Development 121:1833–1844.

Sun Q, Bahri S, Schmid A, Chia W, Zinn K (2000) Receptor tyrosine phosphatases regulate axon guidance across the midline of the *Drosophila* embryo. Development 127:801–812.

Thompson KM, Uetani N, Manitt C, Elchebly M, Tremblay ML, Kennedy TE (2003) Receptor protein tyrosine phosphatase sigma inhibits axonal regeneration and the rate of axon extension. Mol Cell Neurosci 23:681–692.

Tian SS, Tsoulfas P, Zinn K (1991) Three receptor-linked protein-tyrosine phosphatases are selectively expressed on central nervous system axons in the *Drosophila* embryo. Cell 67:675–680.

Tsuchida T, Ensini M, Morton SB, Baldassare M, Edlund T, Jessell TM, Pfaff SL (1994) Topographic organization of embryonic motor neurons defined by expression of LIM homeobox genes. Cell 79:957–970.

Uetani N, Kato K, Ogura H, Mizuno K, Kawano K, Mikoshiba K, Yakura H, Asano M, Iwakura Y (2000) Impaired learning with enhanced hippocampal long-term potentiation in PTPdelta-deficient mice. EMBO J 19:2775–2785.

Van der Zee CE, Man TY, Van Lieshout EM, Van der Heijden I, Van Bree M, Hendriks WJ (2003) Delayed peripheral nerve regeneration and central nervous system collateral sprouting in leucocyte common antigen-related protein tyrosine phosphatase-deficient mice. Eur J Neurosci 17:991–1005.

Van Lieshout EM, Van der Heijden I, Hendriks WJ, Van der Zee CE (2001) A decrease in size and number of basal forebrain cholinergic neurons is paralleled by diminished hippocampal cholinergic innervation in mice lacking leukocyte common antigen-related protein tyrosine phosphatase activity. Neuroscience 102:833–841.

Wallace MJ, Batt J, Fladd CA, Henderson JT, Skarnes W, Rotin D (1999) Neuronal defects and posterior pituitary hypoplasia in mice lacking the receptor tyrosine phosphatase PTPsigma. Nat Genet 21:334–338.

Wills Z, Bateman J, Korey CA, Comer A, Van Vactor D (1999) The tyrosine kinase Abl and its substrate enabled collaborate with the receptor phosphatase Dlar to control motor axon guidance. Neuron 22:301–312.

Xie Y, Yeo TT, Zhang C, Yang T, Tisi MA, Massa SM, Longo FM (2001) The leukocyte common antigen-related protein tyrosine phosphatase receptor regulates regenerative neurite outgrowth *in vivo*. J Neurosci 21:5130–5138.

Yan H, Grossman A, Wang H, D'Eustachio P, Mossie K, Musacchio JM, Silvennoinen O, Schlessinger J (1993) A novel receptor tyrosine phosphatase-sigma that is highly expressed in the nervous system. J Biol Chem 268:24880–24886.

Yeo TT, Yang T, Massa SM, Zhang JS, Honkaniemi J, Butcher LL, Longo FM (1997) Deficient LAR expression decreases basal forebrain cholinergic neuronal size and hippocampal cholinergic innervation. J Neurosci Res 47:348–360.

IL-17 Plays an Important Role in the Development of Experimental Autoimmune Encephalomyelitis[1]

Yutaka Komiyama, Susumu Nakae,[2] Taizo Matsuki,[3] Aya Nambu, Harumichi Ishigame, Shigeru Kakuta, Katsuko Sudo,[4] and Yoichiro Iwakura[5]

IL-17 is a proinflammatory cytokine that activates T cells and other immune cells to produce a variety of cytokines, chemokines, and cell adhesion molecules. This cytokine is augmented in the sera and/or tissues of patients with contact dermatitis, asthma, and rheumatoid arthritis. We previously demonstrated that IL-17 is involved in the development of autoimmune arthritis and contact, delayed, and airway hypersensitivity in mice. As the expression of IL-17 is also augmented in multiple sclerosis, we examined the involvement of this cytokine in these diseases using IL-17$^{-/-}$ murine disease models. We found that the development of experimental autoimmune encephalomyelitis (EAE), the rodent model of multiple sclerosis, was significantly suppressed in IL-17$^{-/-}$ mice; these animals exhibited delayed onset, reduced maximum severity scores, ameliorated histological changes, and early recovery. T cell sensitization against myelin oligodendrocyte glycoprotein was reduced in IL-17$^{-/-}$ mice upon sensitization. The major producer of IL-17 upon treatment with myelin digodendrocyte glycopritein was CD4$^+$ T cells rather than CD8$^+$ T cells, and adoptive transfer of IL-17$^{-/-}$ CD4$^+$ T cells inefficiently induced EAE in recipient mice. Notably, IL-17-producing T cells were increased in IFN-$\gamma^{-/-}$ cells, while IFN-γ-producing cells were increased in IL-17$^{-/-}$ cells, suggesting that IL-17 and IFN-γ mutually regulate IFN-γ and IL-17 production. These observations indicate that IL-17 rather than IFN-γ plays a crucial role in the development of EAE. *The Journal of Immunology,* **2006, 177: 566–573.**

The cytokine IL-17 can activate the expression of a variety of proinflammatory cytokines, chemokines, and cell adhesion molecules throughout a wide range of cell types, including macrophages, dendritic cells, T cells, synovial cells, and endothelial cells (1). Augmented expression of this cytokine is observed in patients with various diseases, such as rheumatoid arthritis (RA)[6] (2), systemic lupus erythematosus (3), Behcet's disease (4), allograft rejection (5), nephritic syndrome (6), asthma (7), and multiple sclerosis (MS) (8), suggesting the involvement of IL-17 in the development of these diseases. We have also demonstrated the contribution of IL-17 to the development of allergic and autoimmune diseases in mice, including contact dermatitis, airway inflammation, and arthritis (9–11). IL-17 also plays an important role in the host defense mechanisms protecting against *Klebsiella pneumoniae* infection (12). However, the role of IL-17 has only been elucidated in a few diseases and the role of this cytokine in the pathogenesis of most diseases remains largely unknown.

IL-17 is produced by a variety of cell types. A subset of Th0 and Th1 cell clones, but not Th2 cell clones, that were established from the synovial tissues of RA patients produced IL-17 (13). A number of Th0, Th1, and Th2 clones established from patients with allergic contact dermatitis also produce this cytokine (14). IL-17 is also produced by TNF-α- and/or GM-CSF-producing CD4$^+$ T cells isolated from the synovial fluid of patients with Lyme arthritis, which exhibit neither a Th1 nor a Th2 phenotype (15). Eosinophils from patients with asthma are also reported to produce this cytokine (16). Both lung neutrophils from mice treated with LPS and CD8$^+$ T cells derived from mice infected with *Klebsiella pneumoniae* are producers of IL-17 (17, 18). Thus, the producer cells of IL-17 differ in a manner dependent on the disease.

Experimental autoimmune encephalomyelitis (EAE), a rodent model of human MS, is induced by immunization of mice with encephalitogenic myelin Ags in the presence of adjuvants. EAE pathogenesis is characterized by inflammation of the CNS associated with demyelination and the infiltration of inflammatory cells including neutrophils and encephalitogenic myelin Ag-specific CD4$^+$ T cells. In MS patients, IL-17 mRNA and protein are increased in both brain lesions and mononuclear cells isolated from blood and cerebrospinal fluids (8, 19). IL-17 is also increased in lymphocytes derived from mice with EAE (20). Although these observations suggest that IL-17 may contribute to the development of MS and EAE, the precise role of this cytokine in the pathogenesis of these diseases is still poorly understood.

In this report, we have investigated the role of IL-17 in the development of the EAE using IL-17$^{-/-}$ mice. We demonstrated that the development of EAE was markedly suppressed in IL-17$^{-/-}$ mice. We also determined that IL-17 was important for the optimal activation of myelin oligodendrocyte glycoprotein

Center for Experimental Medicine, Institute of Medical Science, University of Tokyo, Tokyo, Japan

Received for publication August 30, 2005. Accepted for publication April 7, 2006.

The costs of publication of this article were defrayed in part by the payment of page charges. This article must therefore be hereby marked *advertisement* in accordance with 18 U.S.C. Section 1734 solely to indicate this fact.

[1] This work was supported by grants from the Ministry of Education, Culture, Sports, and Science of Japan, and the Ministry of Health and Welfare of Japan.

[2] Current address: Department of Pathology, Stanford University School of Medicine, 269 Campus Drive, Center for Clinical Sciences Research 3255, Stanford, CA 94305-5176.

[3] Current address: ERATO Yanagisawa Orphan Receptor Project, Japan Science and Technology Agency, Koto-Ku, Japan.

[4] Current address: Animal Research Center, Tokyo Medical University, Sinjyuku-ku, Tokyo 160-8402, Japan.

[5] Address correspondence and reprint requests to Dr. Yoichiro Iwakura, Center for Experimental Medicine, Institute of Medical Science, University of Tokyo, 4-6-1 Shirokanedai, Minato-ku, Tokyo 108-8639, Japan. E-mail address: iwakura@ims.u-tokyo.ac.jp

[6] Abbreviations used in this paper: RA, rheumatoid arthritis; MS, multiple sclerosis; EAE, experimental autoimmune encephalomyelitis; MOG, myelin oligodendrocyte glycoprotein; PTx, pertussis toxin; LN, lymph node; rm, recombinant human; GVHR, graft-vs-host reaction; CIA, collagen-induced arthritis; IDDM, insulin-dependent diabetes mellitus.

0022-1767/06/$02.00

(MOG)-specific T cells. In this model, $CD4^+$ T cells were the major producers of IL-17 in this system.

Materials and Methods

Mice

IL-$17^{-/-}$ mice (9), generated as described previously, were backcrossed to the C57BL/6J strain (six or nine generations). C57BL/6J and IFN-$\gamma^{-/-}$ mice, both on the C57BL/6J background were purchased from Japan SLC and from The Jackson Laboratory, respectively. Mice were kept under pathogen-free conditions in an environmentally controlled clean room at the Center for Experimental Medicine, Institute of Medical Science, University of Tokyo. All experiments were conducted according to the institutional ethical guidelines for animal experimentation and the safety guidelines for genetic manipulation experiments.

Induction of EAE

Active EAE. The MOG_{35-55} peptide (MEVGWYRSPFSRVVHLYRNGK) was synthesized and purified by HPLC at our institute (Dr. S. Imajoh-Ohmi, Division of Molecular Biology, Institute of Medical Science, University of Tokyo). Mice (8–13 wk of age) were immunized s.c. in one flank on day 0 and in the other on day 7 with 300 μg of MOG_{35-55} peptide emulsified in CFA (1:1), which consisted of IFA with 5 mg/ml *Mycobacterium tuberculosis* H37RA (Difco Laboratories). Pertussis toxin (PTx; Alexis) (200 ng) was injected i.v. on days 0 and 2. Following the first immunization, the severity of EAE was monitored and graded on a scale of 0–5: 0, no disease; 1, limp tail; 2, hind limb weakness; 3, hind limb paralysis; 4, hind and fore limb paralysis; 5, moribundity and death.

Passive EAE. Mice were immunized s.c. with MOG/CFA. Ten days after the immunization, the spleen and inguinal and axillary lymph nodes (LNs) were collected and a single-cell suspension was prepared. Pooled lymphocytes (4×10^6 cells/ml) were cultured in the presence of 50 μg/ml MOG_{35-55} peptide in RPMI 1640 medium containing 50 μM 2-ME, 50 μg/ml streptomycin, 50 μg/ml penicillin, and 10% heat-inactivated FBS (Sigma-Aldrich) for 4 days. After harvesting, $CD4^+$ T cells were purified by positive selection using an AutoMACS system (Miltenyi Biotec). Isolated $CD4^+$ T cells (4×10^6) were then transferred i.v. into naive C57BL/6J mice.

Histology

On day 42 after the first immunization with MOG/CFA and PTx, spines were harvested and fixed with neutral 10% formalin. Spinal cords were then extracted and embedded in paraffin. Sections (5 μm) were stained with H&E.

MOG-specific LN cell proliferation assay

Mice were immunized s.c. with MOG/CFA. Ten days after immunization, the inguinal and axillary LNs were collected and a single-cell suspension was prepared. LN cells ($1–4 \times 10^5$ cells/well) were cultured for 72 h in the absence or presence of various concentrations of MOG_{35-55} peptide as described above. Isolated cells were then pulsed for 6 h with [^{3}H]thymidine (0.25 μCi/ml; Amersham Biosciences), and harvested using a Micro 96 cell harvester (Skatron). Levels of radioactivity were measured using a Micro β system (Pharmacia Biotech).

Measurement of cytokine levels by ELISA

To detect IFN-γ and IL-4 in culture supernatants, we used mouse IFN-γ OptEIA kit (BD Pharmingen) and IL-4 ELISA kit (Endogen). Detection of IL-17 by ELISA was performed as described previously (9).

Flow cytometry

To examine LN cell population, inguinal and axillary LN cells were harvested 10 days after immunization with MOG/CFA. After incubation of cells on ice with anti-mouse CD16/CD32 mAb (2.4G2) in a staining buffer (Hank's buffer containing 2% FCS and 0.1% sodium azide) on ice for 15 min, cells were incubated on ice for 45 min with either FITC-anti-mouse CD45RB (C363.16A) or FITC anti-mouse CD62L (MEL-14) in the presence of PE anti-mouse CD44 (Pgp-1) and allophycocyanin anti-mouse CD4 (RM4-5). 7-Aminoactinomycin D (Sigma-Aldrich)-negative, $CD4^+$ cells were examined by a FACSCalibur (BD Biosciences) using CellQuest software (BD Biosciences). To detect IL-17 production in lymphocytes (T cells and B cells), LN cells were harvested 10 days after immunization with MOG/CFA. Isolated cells were cultured in the presence or absence of 50 μg/ml MOG_{35-55} peptide for 72 h as described above. To examine IL-17 production by $Gr\text{-}1^+$ neutrophils, we prepared a single-cell suspension from the spleens of EAE-affected wild-type mice (day 42). LN cells (72 h after cultivation) and spleen cells were stimulated for 6 h with 20 ng/ml PMA (Sigma-Aldrich), 1 μM ionomycin (Sigma-Aldrich), and 2 μM monensin (Sigma-Aldrich) for 6 h. After harvesting, cells were incubated on ice with anti-mouse CD16/CD32 mAb (2.4G2) in a staining buffer on ice for 15 min. Cell samples were then incubated on ice for 45 min with either FITC-anti-mouse B220 (RA3-6B2), FITC anti-mouse Gr-1 (RB6-8C5), or FITC anti-mouse CD3ε (145-2C11), allophycocyanin anti-mouse CD4 (RM4-5 or GK1.5), or allophycocyanin anti-mouse CD8α (53-6.7) Abs. After washing, the cells were fixed in a fixation buffer (2% paraformaldehyde in PBS) at room temperature for 10 min. Samples were then permeabilized with permeabilization buffer (staining buffer containing 0.1% saponin) and incubated for 30 min with PE-conjugated anti-mouse IL-17 mAb (TC11-18H10) or isotype-matched control rat IgG1 (R3-34) at 4°C. The cells were analyzed on a FACSCalibur flow cytometer as described above. All mAbs were purchased from BD Pharmingen.

$CD4^+$ T cell cultures

$CD4^+$ T cells (< 95%) from wild-type mouse spleen were purified by MACS system as described elsewhere (9), then stimulated with 1.0 μg/ml plate-coated anti-CD3 mAb (145-2C11; BD Pharmingen) in the presence or absence of various concentration of recombinant mouse IFN-γ

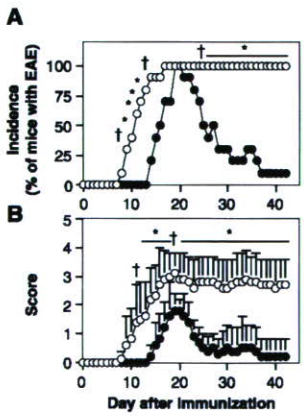

FIGURE 1. Development of EAE was reduced in IL-$17^{-/-}$ mice. EAE was induced in mice by immunization with MOG/CFA coinjected with PTx. *A*, Incidence of EAE. *B*, Clinical scores of diseased mice. ○, Wild-type mice ($n = 10$); ●, IL-$17^{-/-}$ mice ($n = 10$). Data are the averages ± SD for each group. †, $p < 0.05$ and *, $p < 0.001$ vs IL-$17^{-/-}$ mice by Mann-Whitney's U test (*A*) and by χ^2 test (*B*), respectively.

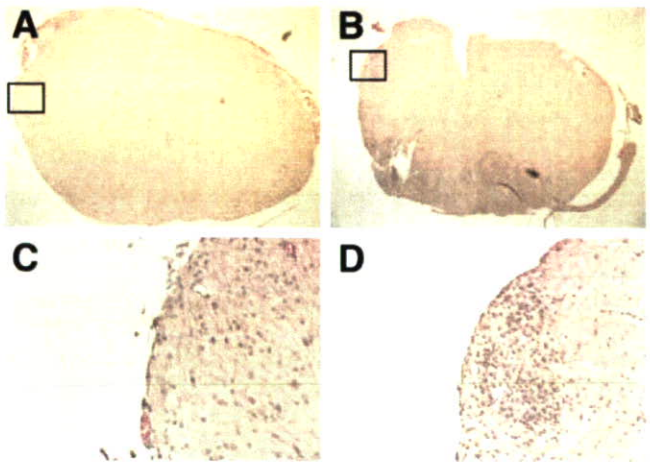

FIGURE 2. Local inflammation of the CNS was suppressed in IL-$17^{-/-}$ mice during EAE. On day 42 after MOG/CFA and PTx immunization, spinal cords were removed. The tissue sections were stained with H&E. The sections at the lumbar level are shown. *A* and *C*, IL-$17^{-/-}$ mice. *B* and *D*, Wild-type mice. *A* and *B*, ×40. *C* and *D*, ×200.

(rmIFN-γ; PeproTech), rmIL-12 (R&D Systems), rmIL-17 (R&D Systems), and rmIL-23 (R&D Systems) for 48 h. Then, culture supernatants were collected and IFN-γ or IL-17 levels in the supernatants were determined by ELISA as described above.

Measurement of MOG-specific serum Ab levels by ELISA

A 96-well flat-bottom plate (Falcon 3912 Micro test III Flexible Assay Plates; BD Biosciences) was coated with 10 μg/ml MOG_{35-55} peptides at 4°C overnight. After washing the wells with 0.05% Tween 20 in PBS, the wells were blocked with PBS containing 1% skim milk, 5 mM EDTA, 0.02% NaN3 for 1 h at room temperature. After washing, diluted serum samples were added and incubated for 2 h at room temperature. Then, after washing the wells, alkaline phosphatase-conjugated goat anti-mouse Igs (IgG, IgG1, IgG2a, IgG2b, IgG3, IgM; Zymed Laboratories) were added and incubated for 1 h at room temperature. Alkaline phosphatase activity was measured using Substrate Phosphatase SIGMA104 (Sigma-Aldrich). The anti-MOG Ab titer was shown as OD_{415} values.

Statistics

The Student *t* test, the Mann-Whitney's *U* test, or the χ^2 test was used for the statistical evaluation of the results.

Results

Development EAE was suppressed in IL-17$^{-/-}$ mice

To investigate the role of IL-17 in the pathogenesis of EAE, we examined the effect of IL-17-deficiency on the development of EAE using IL-17$^{-/-}$ mice. To induce EAE, mice were treated with MOG_{35-55} peptide emulsified in CFA and injected with PTx. The initial signs of EAE were observed 10 days after the first immunization of wild-type mice (Fig. 1). In contrast, the onset of EAE was significantly delayed in IL-17$^{-/-}$ mice until day 15 (Fig. 1). Twenty days after the first immunization, however, IL-17$^{-/-}$ mice exhibited a similar incidence of EAE as that seen in wild-type mice (Fig. 1*A*), although the severity of disease in IL-17$^{-/-}$ mice was milder than that in wild-type mice (Fig. 1*B*). After day 20 from the immunization, the severe signs of disease continued in wild-type mice, while early amelioration was observed in IL-17$^{-/-}$ mice (Fig. 1*A*). Consistent with these observations, a massive infiltration of mononuclear cells was observed within the spinal cords of wild-type mice 42 days after the first immunization (Fig. 2, *B* and *D*). In contrast, the cellular infiltration was significantly reduced in IL-17$^{-/-}$ mice (Fig. 2, *A* and *C*).

PTx is widely used to enhance the development of T cell-mediated organ-specific autoimmune diseases, including EAE. TNF-α$^{-/-}$ mice develop EAE normally when high doses of PTx are injected, while in the presence of low doses of PTx, mutant mice exhibit significantly reduced development of EAE symptoms (21). Thus, PTx may sometimes mask or compensate for the pathological functions of some proinflammatory mediators, such as TNF-α, in the pathogenesis of EAE. Therefore, to more clearly observe the effect of IL-17 deficiency, we next induced EAE in IL-17$^{-/-}$ mice in the absence of PTx treatment. Under these conditions, disease onset in IL-17$^{-/-}$ mice delayed compared with wild-type mice similarly to that seen in the presence of PTx (Fig. 3). Interestingly, in the absence of PTx, the disease also gradually ameliorated in wild-type mice after 22 days of induction, as seen for IL-17$^{-/-}$ mice, although the maximal severity score of the wild-type mice remained significantly higher (Fig. 3). These results demonstrate that IL-17 contributes to the development of EAE.

MOG- specific T cell sensitization was impaired in IL-17$^{-/-}$ mice

We previously showed that IL-17 plays an important role in Ag-specific T cell activation during the development of multiple allergic and autoimmune diseases (9–11). To compare our previous

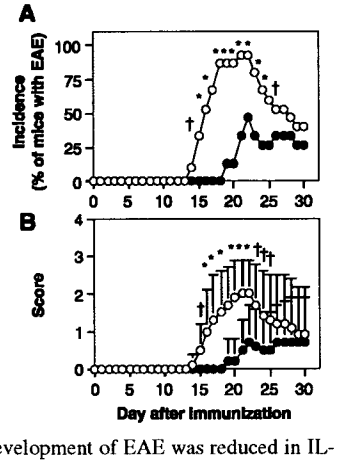

FIGURE 3. Development of EAE was reduced in IL-17$^{-/-}$ mice. Mice were induced EAE by immunization with MOG/CFA, but without PTx. *A*, Incidence of EAE. *B*, Clinical score of diseased mice. ○, Wild-type mice (n = 15), and ●, IL-17$^{-/-}$ mice (n = 15). Data are shown as an average + SD in each group. †, $p < 0.05$ and *, $p < 0.001$ vs IL-17$^{-/-}$ mice by Mann-Whitney's *U* test (*A*) and by χ^2 test (*B*).

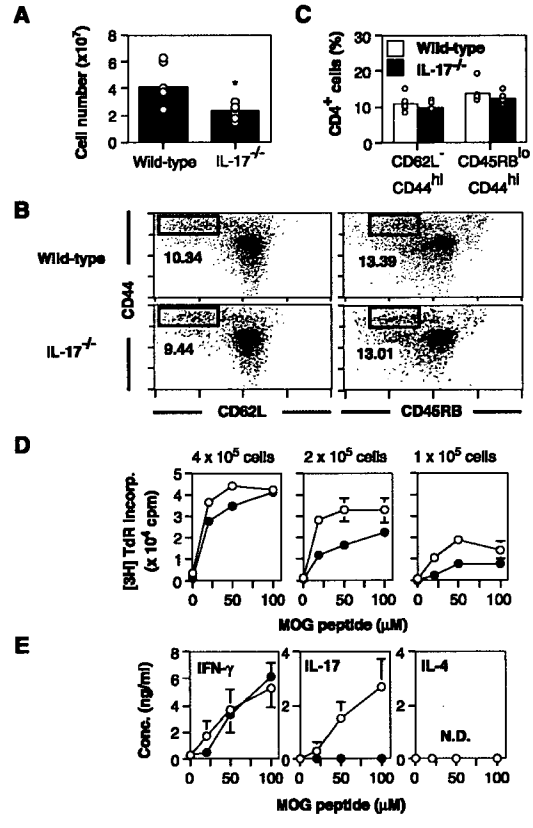

FIGURE 4. MOG-specific lymphocyte activation was impaired in IL-17$^{-/-}$ mice. Mice were immunized once with MOG/CFA in the absence of PTx, and 10 days after immunization, the inguinal and axillary LNs were collected and pooled. *A*, Total LN cell number. *B* and *C*, Percentage of $CD62L^{-}CD44^{high}$ or $CD45RB^{low}CD44^{high}$ $CD4^{+}$ T cells in LNs. In *A* and *C*, each circle represents a value from an individual mouse, and the column represents the average for each group. Representative FACS results are shown in *B*. *, $p < 0.05$ and vs the corresponding values for wild-type mice. *D*, Isolated LN cells were cultured in the absence or presence of MOG peptide for 72 h, and MOG-specific LN cell proliferation as measured by [^{3}H]thymidine incorporation (*D*) and IFN-γ, IL-17, and IL-4 levels in the culture supernatants (2×10^5 cells) (*E*) are shown. ○, Wild-type mice, and ●, IL-17$^{-/-}$ mice. Averages ± SD of triplicate wells are shown. All results are representative at least in three experiments. *D*, Data are averages ± SD from three independent experiments. N.D., Not detected.

results to the models in the current study, we next assessed the role of IL-17 in the activation of MOG-specific T cells during the development of EAE. Ten days after immunization with MOG/CFA alone (without PTx), hypertrophy of inguinal and axillary lymph nodes was observed. Although the total number of pooled inguinal and axillary LN cells was significantly decreased in IL-17$^{-/-}$ mice in comparison with wild-type mice (Fig. 4*A*), the content of memory CD4$^+$ T cells (CD62L$^-$CD44^{high} or CD45RB^{low}CD44^{high}) was comparable (Fig. 4, *B* and *C*). Then, the draining LN cells were cultured in the presence or absence of MOG peptide. When a large excess of LN cells (4×10^5 cells) was present in a well, the observed MOG-specific LN cell proliferative responses in IL-17$^{-/-}$ mice were similar to those seen in wild-type LN cells (Fig. 4*D*). In the presence of an optimal number of LN cells (2×10^5 and 1×10^5 cells), the proliferative responses of cells derived from IL-17$^{-/-}$ mice were markedly decreased compared with those in wild-type mice despite similar number of memory T cells was contained in wild-type and IL-17$^{-/-}$ mouse culture (Fig. 4*D*). IL-17 was detected in the supernatants of wild-type LN cell cultures (2×10^5 cells), and its levels increased in a manner dependent on the dose of MOG peptide. IL-17 was undetectable in IL-17$^{-/-}$ LN cell cultures (2×10^5 cells) (Fig. 4*D*). The MOG-specific proliferative responses of LN T cells were reduced in IL-17$^{-/-}$ mice (Fig. 4D). Nevertheless, IFN-γ production in the LN cell culture supernatants was similar in wild-type and IL-17$^{-/-}$ mice (Fig. 4*E*). IL-4 levels in the LN cell culture supernatants from both wild-type and IL-17$^{-/-}$ mice were below the limit of detection (Fig. 4*E*). These results suggest that the delayed onset of the EAE response in IL-17$^{-/-}$ mice is caused by insufficient T cell sensitization against the MOG peptide.

CD4$^+$ T cells produced IL-17 in LN cells during EAE

Different subsets of CD4$^+$ Th cells and eosinophils are known to produce IL-17 in patients with dermatitis, RA, Lyme arthritis, and asthma (13–16). Neutrophils and CD8$^+$ T cells can also produce IL-17 during certain infectious diseases in mice (17, 18). These observations suggest that the IL-17 producer cells may differ from those known to produce this cytokine in other diseases. Thus, we next analyzed the IL-17 producer cells in the LNs of wild-type mice following MOG immunization. Ten days after immunization, inguinal and axillary LNs were collected and LN cells were cultured in the presence of MOG peptide for 72 h. After MOG stimulation, IL-17 production was detected in CD3$^+$ T cells, but not in granulocytes or B cells (Fig. 5*A*). Within the T cell population, IL-17 was predominantly produced in CD4$^+$ T cells, but at low levels in CD8$^+$ T cells (Fig. 5*B*). Thus, CD4$^+$ T cells, rather than CD8$^+$ T cells, were the major producer of IL-17 within LNs during the development of EAE.

The efficiency of EAE induction of IL-17$^{-/-}$ CD4 T cells was low in comparison with wild-type T cells

To examine the effect of IL-17 deficiency on T cell sensitization against the MOG peptide, we adoptively transferred CD4$^+$ T cells into recipient mice of the same genetic background. Lymphocytes from MOG/CFA-immunized wild-type or IL-17$^{-/-}$ mice were stimulated with MOG peptide for 4 days in vitro, and CD4$^+$ T cells were then purified and transferred into naive wild-type mice. The development of EAE in mice that received IL-17$^{-/-}$ CD4$^+$ T cells was markedly reduced in comparison to those animals receiving wild-type CD4$^+$ T cells (Fig. 6). These observations indicate that MOG-specific T cells from IL-17$^{-/-}$ mice cannot efficiently induce EAE in recipient mice.

IL-17 production was enhanced in IFN-γ$^{-/-}$ mice

MS and EAE are typically classified as Th1 cell-mediated autoimmune diseases. It has been shown, however, that the development of EAE is exacerbated in IFN-γ$^{-/-}$ and/or IFN-γR$^{-/-}$ mice (22–25), indicating that IFN-γ serves a protective role in the disease pathogenesis. Therefore, we next examined whether IFN-γ-deficiency influences IL-17 production by CD4$^+$ T cells during EAE development. Consistent with previous reports, the LN (inguinal and axillary) cell number of IFN-γ$^{-/-}$ mice was significantly increased compared with that of wild-type mice 10 days after MOG/CFA immunization (Fig. 7*A*). When LN cells from MOG-immunized mice were cultured in the presence of MOG peptides, proliferating cells were predominantly observed in a region indicated as "R2", while nonproliferating cells were observed in a region indicated as "R1" (Fig. 7*B*), as determined by CFSE labeling (data not shown). Thus, to detect MOG-reactive, IL-17-producing T cells in LN cells, cells were selectively gated to the R2 region. The percentage of IL-17-producing CD4$^+$ T cells in the draining LN cells of IFN-γ$^{-/-}$ mice was greatly increased in comparison to that in wild-type mouse T cells, irrespective of MOG restimulation (Fig. 7, *C* and *D*). A large proportion of CD8$^+$ T cells, as well as CD4$^+$ T cells from IFN-γ$^{-/-}$ mice immunized with MOG/CFA, produced IL-17, although only a small proportion of CD8$^+$ cells from wild-type mice produced IL-17 (Fig. 7, *C* and *D*).

Next, we assessed the effect of IL-17 on IFN-γ production during MOG immunization. As shown in Fig. 4, *D* and *E*, although MOG-specific T cell proliferation was impaired in IL-17$^{-/-}$ mice, IFN-γ levels in culture supernatants were normally observed. These observations suggested that the IFN-γ-producing cell population is increased in IL-17$^{-/-}$ mice. In support of this, the percentage of IFN-γ-producing CD4$^+$ T cells in the draining LN cells

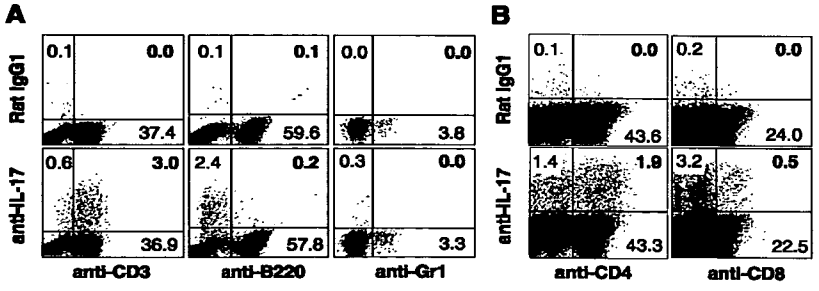

FIGURE 5. IL-17 was primarily produced by CD4$^+$ LN T cells during the development of EAE. To detect IL-17-producing cells in the lymphocyte or granulocyte populations, LN cells from mice immunized with MOG/CFA were cultured in the presence of 50 μg/ml MOG peptide for 72 h, followed by stimulation with PMA + ionomycin in the presence of monensin; then IL-17-producing cells were detected by FACS. Gr-1$^+$ cells were stained using spleen cells from mice with EAE. *A*, The IL-17$^+$ populations in CD3$^+$ or B220$^+$ cell populations within the LN cells, or the Gr-1$^+$ cells of the spleen. *B*, IL-17 production by CD3$^+$CD4$^+$ or CD3$^+$CD8$^+$ T cells.

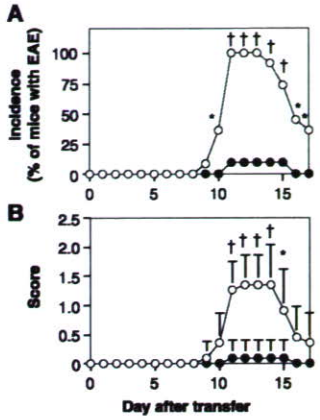

FIGURE 6. $CD4^+$ T cells were responsible for the induction of EAE. Mice were immunized once with MOG/CFA alone. At 10 days postimmunization, the spleen and the inguinal and axillary LNs were collected and pooled. The pooled cells were cultured in the presence of MOG peptide for 72 h, and then $CD4^+$ T cells were purified and transferred into naive, wild-type mice. *A*, The incidence of EAE. *B*, The clinical scores of the diseased mice. ○, Mice that received wild-type $CD4^+$ T cells ($n = 11$), and, ●, mice that received IL-$17^{-/-}$ $CD4^+$ T cells ($n = 10$). In *B*, data are shown as the averages ± SD for each group. †, $p < 0.05$ and *, $p < 0.001$ vs IL-$17^{-/-}$ mice by the Mann-Whitney's *U* test (*A*) and by the χ^2 test (*B*), respectively.

of IL-$17^{-/-}$ mice was significantly increased compared with that in wild-type mice after MOG stimulation (Fig. 8). Similar results were also obtained in $CD8^+$ T cells (Fig. 8). Thus, these data suggest that IL-17 production is regulated by IFN-γ while IFN-γ is regulated by IL-17.

Then, we examined whether IL-17 and IFN-γ can directly regulate IFN-γ and IL-17 production, respectively. When purified splenic $CD4^+$ T cells were stimulated with plate-coated anti-CD3 mAb in the presence of various concentration of IL-12, IFN-γ production was enhanced in a dose-dependent manner (Fig. 9*A*). However, IL-17 did not influence IFN-γ production by $CD4^+$ T cells in the absence or presence of IL-12 (Fig. 9, *B* and *C*). IL-23 could promote IL-17 production dose dependently (Fig. 9*D*), while IFN-γ did not show any effects on IL-17 production irrespective of the presence of IL-23 (Fig. 9, *E* and *F*). These observations indicate that IFN-γ or IL-17 cannot directly modulate IL-17 or IFN-γ production.

Increased MOG-specific Ab production in IL-$17^{-/-}$ mice during EAE

To elucidate the role of IL-17 in MOG-specific Ab production, we measured the level of anti-MOG-specific serum Abs in wild-type and IL-$17^{-/-}$ mice during EAE. Before immunization with MOG peptides, the level of MOG-specific IgG was very low in both wild-type and IL-$17^{-/-}$ mice (Fig. 10*A*). On day 20 after MOG/CFA immunization with PTx injection as shown in Fig. 1, the level of MOG-specific IgG in IL-$17^{-/-}$ mice was slightly higher than that in wild-type mice (Fig. 10*A*). In chronic inflammatory phases during EAE induced by MOG/CFA with PTx, the levels of MOG-specific IgG and IgG1 in IL-$17^{-/-}$ mice were profoundly increased compared with these in wild-type mice, although these IL-$17^{-/-}$ mice did not show any sign of EAE (Fig. 10). Similarly, the levels of MOG-specific IgG2a and IgG2b were also slightly, but not significantly, increased in IL-$17^{-/-}$ mice, while those of MOG-specific IgG3 and IgM were not different between wild-type and IL-$17^{-/-}$ mice (Fig. 10*B*). These results indicated that IL-17 has an influence upon MOG-specific Ab production by B cells.

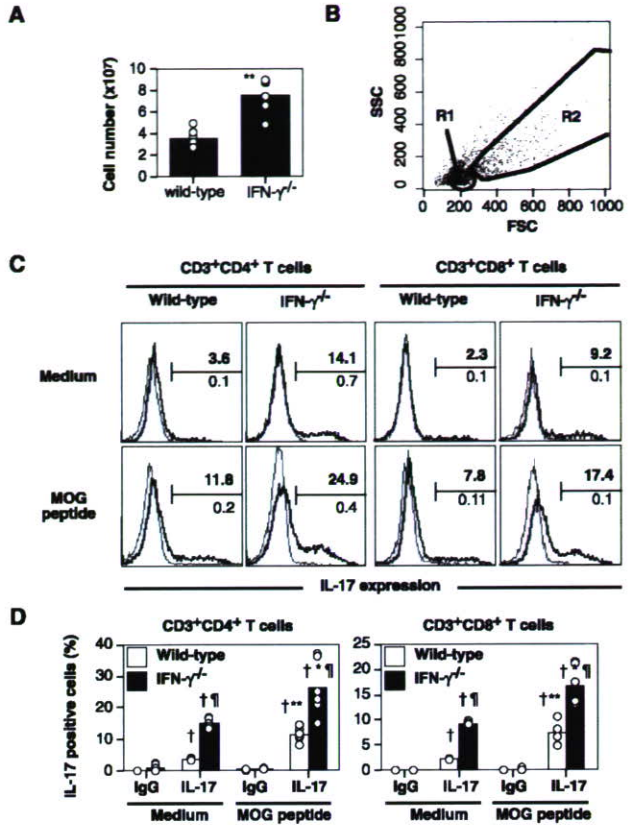

FIGURE 7. The proportion of IL-17-producing $CD4^+$ and $CD8^+$ T cells was increased in IFN-$\gamma^{-/-}$ mice after MOG immunization. LN cells from mice immunized with MOG/CFA were cultured for 72 h in the presence or absence of 50 μg/ml MOG peptide. IL-17-producing cells were then analyzed by FACS, and the percentage of IL-$17^+CD3^+CD4^+$ T cells is shown. *A*, Total LN cell number from inguinal and axillary LNs from wild-type ($n = 6$) and IFN-$\gamma^{-/-}$ ($n = 6$) mice. **, $p < 0.01$ vs wild-type mice. *B*, Gating in FACS analysis, R2 rather than R1 contained MOG-specific proliferating cells using CFSE labeling. *C*, Staining of intracellular IL-17 in $CD3^+CD4^+$ or $CD3^+CD8^+$ T cells stimulated with or without MOG peptides. Shaded areas, staining with isotype-matched control Ab; bold lines, anti-mouse IL-17 staining. The percentage of IL-17-positive cells (upper bold figures) and percentage of cells which were stained with an isotype-matched control IgG (lower figures) are shown. *D*, Each circle represents a value from an individual mouse, and the column represents the average for each group in *C*. □, Wild-type mice ($n = 6$). ■, IFN-$\gamma^{-/-}$ mice ($n = 6$). IgG, isotype-matched control IgG staining. IL-17, anti-mouse IL-17 staining. †, $p < 0.05$ vs the corresponding values for control IgG staining. *, $p < 0.05$ and **, $p < 0.01$ vs the corresponding values for the cultures in the absence of MOG peptide (medium alone). ¶, $p < 0.05$ vs the corresponding values of wild-type mice. All *p* values were determined by the Student's *t* test.

However, our findings suggest that no correlation exists between the susceptibility and severity of EAE and the levels of anti-MOG Abs in IL-$17^{-/-}$ mice.

Discussion

In this study, we have demonstrated using IL-$17^{-/-}$ mice that IL-17 plays an important role in the development of EAE induced by MOG/CFA. We found that, upon immunization with MOG/CFA, T cell sensitization was defective in IL-$17^{-/-}$ mice, and $CD4^+$ T cells from IL-$17^{-/-}$ mice did not induce EAE efficiently compared with wild-type T cells. These observations suggest that IL-17 plays an important role in the activation of encephalitogenic T cells during the sensitization phase of EAE. In contrast, it was recently reported that IL-17-producing $CD4^+$ T cells enhance the

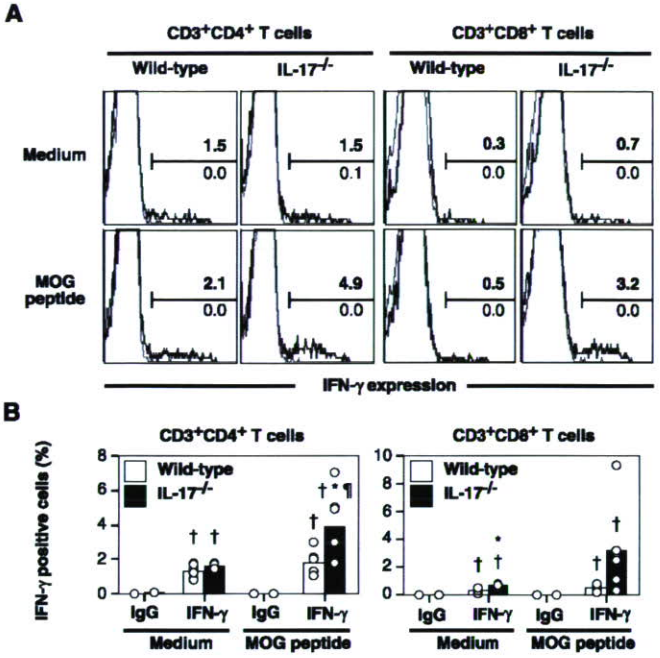

FIGURE 8. The proportion of IFN-γ-producing $CD4^+$ and $CD8^+$ T cells was increased in IL-$17^{-/-}$ mice after MOG immunization. LN cells from mice immunized with MOG/CFA were cultured for 72 h in the presence or absence of 50 μg/ml MOG peptide. IFN-γ-producing cells were then analyzed by FACS, and the percentage of IFN-$\gamma^+CD3^+CD4^+$ or $CD3^+CD8^+$ T cells is shown. *A*, Staining of intracellular IFN-γ in $CD3^+CD4^+$ or $CD3^+CD8^+$ T cells stimulated with or without MOG peptides. Shaded areas, staining with isotype-matched control Ab; bold lines, anti-mouse IFN-γ staining. The percentage of IFN-γ-positive cells (upper bold figures) and percentage of cells which were stained with an isotype-matched control IgG (lower figures) are shown. *B*, Each circle represents a value from an individual mouse, and the column represents the average for each group in *A*. □, Wild-type mice ($n = 6$). ■, IL-$17^{-/-}$ mice ($n = 6$). IgG, isotype-matched control IgG staining. IFN-γ, anti-mouse IFN-γ staining. †, $p < 0.05$ vs the corresponding values for control IgG staining. *, $p < 0.05$ vs the corresponding values for the cultures in the absence of MOG peptide (medium alone). ¶, $p < 0.05$ vs the corresponding values of wild-type mice. All p values were determined by the Student t test.

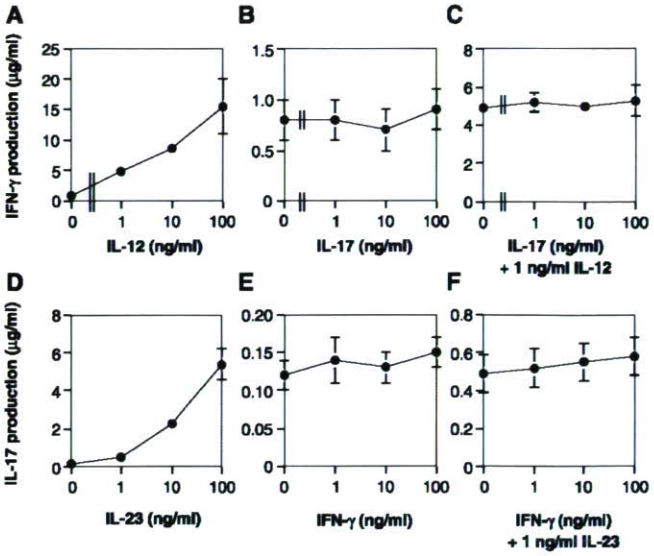

FIGURE 9. Exogenous IFN-γ and IL-17 did not directly affect IL-17 and IFN-γ production by $CD4^+$ T cells. $CD4^+$ T cells from spleen of wild-type mice were stimulated with plate-coated anti-CD3 mAb in the presence or absence of rmIL-17 or rmIFN-γ with or without rmIL-12 or rmIL-23 for 48 h. Then, IFN-γ or IL-17 levels in culture supernatants were determined by ELISA. IFN-γ levels in culture supernatants from $CD4^+$ T cells: stimulated with anti-CD3 mAb plus the indicated amount of rmIL-12 (*A*), rmIL-17 (*B*), and 1 ng/ml rmIL-12 + indicated amount of rmIL-17 (*C*). IL-17 levels in culture supernatants from $CD4^+$ T cells: stimulated with anti-CD3 mAb plus rmIL-23 (*D*), rmIFN-γ (*E*), or 1 ng/ml rmIL-23 + indicated amount of rmIFN-γ (*F*). Data showed the average ± SD from three mice, and a representative result from two independent experiments.

disease severity of EAE and that treatment with anti-IL-17 neutralizing Abs during the elicitation phase suppressed disease development (26). These observations strongly suggest that IL-17 is involved in the pathogenesis of EAE during both the sensitization and elicitation phases.

As Th1 cells, which are the major producers of IFN-γ, infiltrate the inflamed lesions of EAE or collagen-induced arthritis (CIA) (27, 28), it was suspected that IFN-γ may have a pathological role in the development of these autoimmune diseases. However, administration of neutralizing Abs for IFN-γ leads to exacerbation of these diseases (29). The development of CIA is enhanced in IFN-$\gamma^{-/-}$ mice and that of EAE is also exacerbated in both IFN-$\gamma^{-/-}$ and IFN-$\gamma R^{-/-}$ mice compared with wild-type mice (22–25). Thus, IFN-γ may have a protective role in these diseases, rather than a pathogenic role. Consistent with this notion, the development of EAE is also exacerbated in mice deficient for IL-12 p35, a subunit of IL-12 that is required for the differentiation of IFN-γ-producing Th1 cells (30, 31). In a similar manner, the severity of EAE was exaggerated in mice deficient in IL-12Rβ2. Interestingly, we found that the IL-17-producing T cell population was increased in IFN-$\gamma^{-/-}$ mice in comparison to that seen in wild-type mice upon immunized with MOG/CFA (Fig. 7). Similar observations were also currently reported by other groups (32, 33). IL-17 production was also augmented in the splenocytes of IL-12Rβ$2^{-/-}$ mice (20). These observations suggest that IFN-γ plays a beneficial role during the development of EAE by regulating IL-17 production. However, we demonstrated that IFN-γ did not directly influence IL-17 production by $CD4^+$ T cells (Fig. 9, *E* and *F*), suggesting that the suppressive effect of IFN-γ on IL-17 production may be due to the suppression of the development of IL-17-producing cells. In this context, it was recently reported that IL-17-producing cells are induced by IL-23, while IL-12/IFN-γ suppresses the production of IL-17 (34).

We also found that IFN-γ-producing $CD4^+$ and $CD8^+$ T cells were markedly increased in IL-$17^{-/-}$ mice stimulated with MOG peptides, although IL-17 did not show any direct effect on IFN-γ production by $CD4^+$ T cells (Fig. 9, *B* and *C*) (Fig. 8). These observations suggest that IL-17 negatively regulates the development of IFN-γ-producing Th1 cells. Thus, IL-17 and IFN-γ may mutually regulate the development of these cytokine producer cells during immune responses.

We demonstrated that $CD4^+$ T cells are the predominant producers of IL-17 in LN cells after immunization with MOG/CFA. It has been reported that, in Lyme arthritis, IL-17 is primarily produced by a specific subpopulation of $CD4^+$ T cells that are neither Th1 nor Th2 and that produce TNF-α and/or GM-CSF simultaneously. As IL-17 is produced by multiple cell types, including $CD8^+$ T cells, γδ T cells, neutrophils, and eosinophils under different conditions (13–18, 35), the production of IL-17 is not limited to a specific T cell population. Instead, the producer cells in a particular disease appear to be defined by a specific cell population. The mechanism by which these IL-17 producer cells are controlled in different diseases, however, remains to be elucidated.

In MS patients, elevation of anti-MOG Ab levels is detectable in cerebrospinal fluid (36, 37). In association with the elevation of

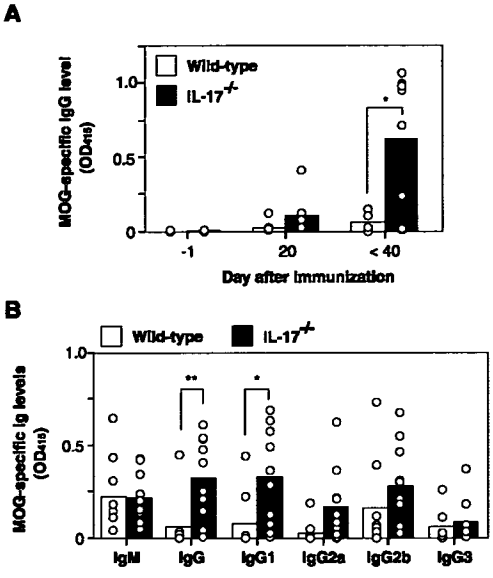

FIGURE 10. Enhanced MOG-specific Ig production in IL-17$^{-/-}$ mice during EAE. MOG-specific Ig levels in sera from wild-type and IL-17$^{-/-}$ mice that developed EAE were determined by ELISA. *A*, As performed in Fig. 1*A*, sera were collected from mice before (−1 day) and after MOG immunization (20 and <40 days). Then, MOG-specific IgG levels in sera were measured. *B*, On day 42 after MOG immunization, MOG-specific IgM, IgG, IgG1, IgG2a, IgG2b, and IgG3 levels in sera were determined. Each circle represents the value from an individual mouse, and a column shows the average of each group. □, Wild-type mice (n = 7). ■, IL-17$^{-/-}$ mice (n = 10). *, $p < 0.05$ and **, $p < 0.01$ for the comparisons shown in brackets by Student's t test.

anti-MOG Abs following immunization with MOG peptides (38), severe demyelination occurred in the Lewis rat, suggesting that the generation of myelin-specific Abs may be involved in the development of EAE. However, we observed that anti-MOG Ab levels were increased in IL-17$^{-/-}$ mice in comparison with the levels seen in wild-type mice after immunization with MOG, while the development of EAE was markedly suppressed in IL-17$^{-/-}$ mice (Fig. 10). Thus, in IL-17$^{-/-}$ mice, there is no apparent correlation between the severity of EAE and the elevation of anti-MOG Abs in IL-17$^{-/-}$ mice, suggesting that anti-MOG Abs are not directly involved in the development of this disease. In fact, the serum MOG-specific Ab levels in mice that developed EAE after the transfer of MOG-specific CD4$^+$ T cells were below the limits of detection (data not shown). In support of this notion, B cell-deficient mice develop EAE normally (39–41). It was reported, however, that Abs are involved in the remyelination of the lesions in the CNS during disease resolution (42). We did not expect that Ab levels specific for MOG would be enhanced in IL-17$^{-/-}$ mice, because Ab production was suppressed in IL-17$^{-/-}$ mice during CIA and contact, delayed-type, and airway hypersensitivity (9–11). We do not currently understand the reasoning for this. The molecular nature of the Ags involved in the autoimmune disorders, however, appears to affect the sensitivity of the disease to IL-17. Additional experiments will be necessary to elucidate the mechanism.

We previously reported that IL-17 is not essential for the induction of graft-vs-host reaction (GVHR) (9), in which CD8$^+$ T cell-derived FasL and perforin play important roles (43, 44). Likewise, IL-17-deficiency did not affect the incidence of hyperglycemia in NOD mice (T. Matsuki, S. Nakae, and Y. Iwakura, unpublished observations), although IL-17 mRNA expression is increased in NOD mice upon development of insulin-dependent diabetes mellitus (IDDM) (45). In this case, CD8$^+$ cells, rather than CD4$^+$ cells, are also suggested to be involved in the apoptosis of β cells in the pancreatic Langerhans islands (46, 47). In both cases, IFN-γ is involved in the pathogenesis of the diseases (48, 49) (50). Thus, these observations indicate that these two types of inflammatory responses are clearly different; EAE and CIA are IL-17 dependent, and IL-17-producing cells play a major role, while IDDM and GVHR are IFN-γ dependent, and CD8$^+$ cytotoxic T cells and/or CD4$^+$ Th1 cells play important roles.

Taken together, our data demonstrate that IL-17 and IFN-γ, produced by a distinct population of T cells, have different roles in the development of EAE, CIA, GVHR, and hyperglycemia. These results suggest that these cytokines may also be involved in the development of MS, RA, GVHD, and IDDM in humans. Elucidation of the roles of pathogenic cytokines and the mechanisms of cytokine dependency may provide potential targets for novel therapeutics to treat these diseases.

Acknowledgments

We thank Dr. S. J. Galli (Stanford University School of Medicine, Stanford, CA) for his generous support for this study. We also thank Tomoko Hata and Hayato Kotaki for their excellent animal care.

Disclosures

The authors have no financial conflict of interest.

References

1. Moseley, T. A., D. R. Haudenschild, L. Rose, and A. H. Reddi. 2003. Interleukin-17 family and IL-17 receptors. *Cytokine Growth Factor Rev.* 14: 155–174.
2. Chabaud, M., J. M. Durand, N. Buchs, F. Fossiez, G. Page, L. Frappart, and P. Miossec. 1999. Human interleukin-17: A T cell-derived proinflammatory cytokine produced by the rheumatoid synovium. *Arthritis Rheum.* 42: 963–970.
3. Wong, C. K., C. Y. Ho, E. K. Li, and C. W. Lam. 2000. Elevation of proinflammatory cytokine (IL-18, IL-17, IL-12) and Th2 cytokine (IL-4) concentrations in patients with systemic lupus erythematosus. *Lupus* 9: 589–593.
4. Hamzaoui, K., A. Hamzaoui, F. Guemira, M. Bessioud, M. Hamza, and K. Ayed. 2002. Cytokine profile in Behcet's disease patients: relationship with disease activity. *Scand. J. Rheumatol.* 31: 205–210.
5. Antonysamy, M. A., W. C. Fanslow, F. Fu, W. Li, S. Qian, A. B. Troutt, and A. W. Thomson. 1999. Evidence for a role of IL-17 in organ allograft rejection: IL-17 promotes the functional differentiation of dendritic cell progenitors. *J. Immunol.* 162: 577–584.
6. Matsumoto, K., and K. Kanmatsuse. 2002. Increased urinary excretion of interleukin-17 in nephrotic patients. *Nephron* 91: 243–249.
7. Wong, C. K., C. Y. Ho, F. W. Ko, C. H. Chan, A. S. Ho, D. S. Hui, and C. W. Lam. 2001. Proinflammatory cytokines (IL-17, IL-6, IL-18 and IL-12) and Th cytokines (IFN-γ, IL-4, IL-10 and IL-13) in patients with allergic asthma. *Clin. Exp. Immunol.* 125: 177–183.
8. Lock, C., G. Hermans, R. Pedotti, A. Brendolan, E. Schadt, H. Garren, A. Langer-Gould, S. Strober, B. Cannella, J. Allard, et al. 2002. Gene-microarray analysis of multiple sclerosis lesions yields new targets validated in autoimmune encephalomyelitis. *Nat. Med.* 8: 500–508.
9. Nakae, S., Y. Komiyama, A. Nambu, K. Sudo, M. Iwase, I. Homma, K. Sekikawa, M. Asano, and Y. Iwakura. 2002. Antigen-specific T cell sensitization is impaired in IL-17-deficient mice, causing suppression of allergic cellular and humoral responses. *Immunity* 17: 375–387.
10. Nakae, S., A. Nambu, K. Sudo, and Y. Iwakura. 2003. Suppression of immune induction of collagen-induced arthritis in IL-17-deficient mice. *J. Immunol.* 171: 6173–6177.
11. Nakae, S., S. Saijo, R. Horai, K. Sudo, S. Mori, and Y. Iwakura. 2003. IL-17 production from activated T cells is required for the spontaneous development of destructive arthritis in mice deficient in IL-1 receptor antagonist. *Proc. Natl. Acad. Sci. USA* 100: 5986–5990.
12. Ye, P., F. H. Rodriguez, S. Kanaly, K. L. Stocking, J. Schurr, P. Schwarzenberger, P. Oliver, W. Huang, P. Zhang, J. Zhang, et al. 2001. Requirement of interleukin 17 receptor signaling for lung CXC chemokine and granulocyte colony-stimulating factor expression, neutrophil recruitment, and host defense. *J. Exp. Med.* 194: 519–527.
13. Aarvak, T., M. Chabaud, P. Miossec, and J. B. Natvig. 1999. IL-17 is produced by some proinflammatory Th1/Th0 cells but not by Th2 cells. *J. Immunol.* 162: 1246–1251.
14. Albanesi, C., C. Scarponi, A. Cavani, M. Federici, F. Nasorri, and G. Girolomoni. 2000. Interleukin-17 is produced by both Th1 and Th2 lymphocytes, and modulates interferon-γ- and interleukin-4-induced activation of human keratinocytes. *J. Invest. Dermatol.* 115: 81–87.
15. Infante-Duarte, C., H. F. Horton, M. C. Byrne, and T. Kamradt. 2000. Microbial lipopeptides induce the production of IL-17 in Th cells. *J. Immunol.* 165: 6107–6115.

16. Molet, S., Q. Hamid, F. Davoine, E. Nutku, R. Taha, N. Page, R. Olivenstein, J. Elias, and J. Chakir. 2001. IL-17 is increased in asthmatic airways and induces human bronchial fibroblasts to produce cytokines. *J. Allergy Clin. Immunol.* 108: 430–438.
17. Ferretti, S., O. Bonneau, G. R. Dubois, C. E. Jones, and A. Trifilieff. 2003. IL-17, produced by lymphocytes and neutrophils, is necessary for lipopolysaccharide-induced airway neutrophilia: IL-15 as a possible trigger. *J. Immunol.* 170: 2106–2112.
18. Happel, K. I., M. Zheng, E. Young, L. J. Quinton, E. Lockhart, A. J. Ramsay, J. E. Shellito, J. R. Schurr, G. J. Bagby, S. Nelson, and J. K. Kolls. 2003. Roles of Toll-like receptor 4 and IL-23 in IL-17 expression in response to *Klebsiella pneumoniae* infection. *J. Immunol.* 170: 4432–4436.
19. Matusevicius, D., P. Kivisakk, B. He, N. Kostulas, V. Ozenci, S. Fredrikson, and H. Link. 1999. Interleukin-17 mRNA expression in blood and CSF mononuclear cells is augmented in multiple sclerosis. *Mult. Scler.* 5: 101–104.
20. Zhang, G. X., B. Gran, S. Yu, J. Li, I. Siglienti, X. Chen, M. Kamoun, and A. Rostami. 2003. Induction of experimental autoimmune encephalomyelitis in IL-12 receptor-β2-deficient mice: IL-12 responsiveness is not required in the pathogenesis of inflammatory demyelination in the central nervous system. *J. Immunol.* 170: 2153–2160.
21. Kassiotis, G., K. Kranidioti, and G. Kollias. 2001. Defective CD4T cell priming and resistance to experimental autoimmune encephalomyelitis in TNF-deficient mice due to innate immune hypo-responsiveness. *J. Neuroimmunol.* 119: 239–247.
22. Ferber, I. A., S. Brocke, C. Taylor-Edwards, W. Ridgway, C. Dinisco, L. Steinman, D. Dalton, and C. G. Fathman. 1996. Mice with a disrupted IFN-γ gene are susceptible to the induction of experimental autoimmune encephalomyelitis (EAE). *J. Immunol.* 156: 5–7.
23. Willenborg, D. O., S. Fordham, C. C. Bernard, W. B. Cowden, and I. A. Ramshaw. 1996. IFN-γ plays a critical down-regulatory role in the induction and effector phase of myelin oligodendrocyte glycoprotein-induced autoimmune encephalomyelitis. *J. Immunol.* 157: 3223–3227.
24. Chu, C. Q., S. Wittmer, and D. K. Dalton. 2000. Failure to suppress the expansion of the activated CD4 T cell population in interferon γ-deficient mice leads to exacerbation of experimental autoimmune encephalomyelitis. *J. Exp. Med.* 192: 123–128.
25. Krakowski, M., and T. Owens. 1996. Interferon-γ confers resistance to experimental allergic encephalomyelitis. *Eur. J. Immunol.* 26: 1641–1646.
26. Langrish, C. L., Y. Chen, W. M. Blumenschein, J. Mattson, B. Basham, J. D. Sedgwick, T. McClanahan, R. A. Kastelein, and D. J. Cua. 2005. IL-23 drives a pathogenic T cell population that induces autoimmune inflammation. *J. Exp. Med.* 201: 233–240.
27. Traugott, U., and P. Lebon. 1988. Demonstration of α, β, and γ interferon in active chronic multiple sclerosis lesions. *Ann. NY Acad. Sci.* 540: 309–311.
28. Hammarberg, H., O. Lidman, C. Lundberg, S. Y. Eltayeb, A. W. Gielen, S. Muhallab, A. Svenningsson, H. Linda, P. H. van Der Meide, S. Cullheim, et al. 2000. Neuroprotection by encephalomyelitis: rescue of mechanically injured neurons and neurotrophin production by CNS-infiltrating T and natural killer cells. *J. Neurosci.* 20: 5283–5291.
29. Begolka, W. S., and S. D. Miller. 1998. Cytokines as intrinsic and exogenous regulators of pathogenesis in experimental autoimmune encephalomyelitis. *Res. Immunol.* 149: 771–781; discussion 843; 774: 855–760.
30. Becher, B., B. G. Durell, and R. J. Noelle. 2002. Experimental autoimmune encephalitis and inflammation in the absence of interleukin-12. *J. Clin. Invest.* 110: 493–497.
31. Gran, B., G. X. Zhang, S. Yu, J. Li, X. H. Chen, E. S. Ventura, M. Kamoun, and A. Rostami. 2002. IL-12p35-deficient mice are susceptible to experimental autoimmune encephalomyelitis: evidence for redundancy in the IL-12 system in the induction of central nervous system autoimmune demyelination. *J. Immunol.* 169: 7104–7110.
32. Park, H., Z. Li, X. O. Yang, S. H. Chang, R. Nurieva, Y. H. Wang, Y. Wang, L. Hood, Z. Zhu, Q. Tian, and C. Dong. 2005. A distinct lineage of CD4 T cells regulates tissue inflammation by producing interleukin 17. *Nat. Immunol.* 6: 1133–1141.
33. Harrington, L. E., R. D. Hatton, P. R. Mangan, H. Turner, T. L. Murphy, K. M. Murphy, and C. T. Weaver. 2005. Interleukin 17-producing CD4$^+$ effector T cells develop via a lineage distinct from the T helper type 1 and 2 lineages. *Nat. Immunol.* 6: 1123–1132.
34. Aggarwal, S., N. Ghilardi, M. H. Xie, F. J. de Sauvage, and A. L. Gurney. 2003. Interleukin-23 promotes a distinct CD4 T cell activation state characterized by the production of interleukin-17. *J. Biol. Chem.* 278: 1910–1914.
35. Umemura, M., T. Kawabe, K. Shudo, H. Kidoya, M. Fukui, M. Asano, Y. Iwakura, G. Matsuzaki, R. Imamura, and T. Suda. 2004. Involvement of IL-17 in Fas ligand-induced inflammation. *Int. Immunol.* 16: 1099–1108.
36. Xiao, B. G., C. Linington, and H. Link. 1991. Antibodies to myelin-oligodendrocyte glycoprotein in cerebrospinal fluid from patients with multiple sclerosis and controls. *J. Neuroimmunol.* 31: 91–96.
37. Sun, J., H. Link, T. Olsson, B. G. Xiao, G. Andersson, H. P. Ekre, C. Linington, and P. Diener. 1991. T and B cell responses to myelin-oligodendrocyte glycoprotein in multiple sclerosis. *J. Immunol.* 146: 1490–1495.
38. Ichikawa, M., T. G. Johns, J. Liu, and C. C. Bernard. 1996. Analysis of the fine B cell specificity during the chronic/relapsing course of a multiple sclerosis-like disease in Lewis rats injected with the encephalitogenic myelin oligodendrocyte glycoprotein peptide 35–55. *J. Immunol.* 157: 919–926.
39. Wolf, S. D., B. N. Dittel, F. Hardardottir, and C. A. Janeway, Jr. 1996. Experimental autoimmune encephalomyelitis induction in genetically B cell-deficient mice. *J. Exp. Med.* 184: 2271–2278.
40. Hjelmstrom, P., A. E. Juedes, J. Fjell, and N. H. Ruddle. 1998. B-cell-deficient mice develop experimental allergic encephalomyelitis with demyelination after myelin oligodendrocyte glycoprotein sensitization. *J. Immunol.* 161: 4480–4483.
41. Dittel, B. N., T. H. Urbania, and C. A. Janeway, Jr. 2000. Relapsing and remitting experimental autoimmune encephalomyelitis in B cell deficient mice. *J. Autoimmun.* 14: 311–318.
42. Hunter, S. F., D. J. Miller, and M. Rodriguez. 1997. Monoclonal remyelination-promoting natural autoantibody SCH 94.03: pharmacokinetics and in vivo targets within demyelinated spinal cord in a mouse model of multiple sclerosis. *J. Neurol. Sci.* 150: 103–113.
43. Baker, M. B., N. H. Altman, E. R. Podack, and R. B. Levy. 1996. The role of cell-mediated cytotoxicity in acute GVHD after MHC-matched allogeneic bone marrow transplantation in mice. *J. Exp. Med.* 183: 2645–2656.
44. Brochu, S., B. Rioux-Masse, J. Roy, D. C. Roy, and C. Perreault. 1999. Massive activation-induced cell death of alloreactive T cells with apoptosis of bystander postthymic T cells prevents immune reconstitution in mice with graft-versus-host disease. *Blood* 94: 390–400.
45. Vukkadapu, S. S., J. M. Belli, K. Ishii, A. G. Jegga, J. J. Hutton, B. J. Aronow, and J. D. Katz. 2005. Dynamic interaction between T cell-mediated β cell damage and β cell repair in the run-up to autoimmune diabetes of the NOD mouse. *Physiol. Genomics* 21: 201–211.
46. Kagi, D., B. Odermatt, P. Seiler, R. M. Zinkernagel, T. W. Mak, and H. Hengartner. 1997. Reduced incidence and delayed onset of diabetes in perforin-deficient nonobese diabetic mice. *J. Exp. Med.* 186: 989–997.
47. Itoh, N., A. Imagawa, T. Hanafusa, M. Waguri, K. Yamamoto, H. Iwahashi, M. Moriwaki, H. Nakajima, J. Miyagawa, M. Namba, et al. 1997. Requirement of Fas for the development of autoimmune diabetes in nonobese diabetic mice. *J. Exp. Med.* 186: 613–618.
48. Hultgren, B., X. Huang, N. Dybdal, and T. A. Stewart. 1996. Genetic absence of γ-interferon delays but does not prevent diabetes in NOD mice. *Diabetes* 45: 812–817.
49. Wang, B., I. Andre, A. Gonzalez, J. D. Katz, M. Aguet, C. Benoist, and D. Mathis. 1997. Interferon-γ impacts at multiple points during the progression of autoimmune diabetes. *Proc. Natl. Acad. Sci. USA* 94: 13844–13849.
50. Ellison, C. A., J. M. Fischer, K. T. HayGlass, and J. G. Gartner. 1998. Murine graft-versus-host disease in an F_1-hybrid model using IFN-γ gene knockout donors. *J. Immunol.* 161: 631–640.

changes at or near promoters, whereas TopoI inhibitors caused transcription complexes to stall in the midst of transcription units (*34*).

Collectively, our data reveal that a transient dsDNA break occurs at multiple regulated transcription units. This raises questions regarding the interplay between molecular machineries that are involved in the repair of dsDNA breaks and the activation of the gene transcription.

References and Notes

1. C. K. Glass, M. G. Rosenfeld, *Genes Dev.* **14**, 121 (2000).
2. B. M. Spiegelman, R. Heinrich, *Cell* **119**, 157 (2004).
3. V. Perissi, M. G. Rosenfeld, *Nat. Rev. Mol. Cell Biol.* **6**, 542 (2005).
4. A. Tulin, D. Stewart, A. C. Spradling, *Genes Dev.* **16**, 2108 (2002).
5. R. Pavri *et al.*, *Mol. Cell* **18**, 83 (2005).
6. M. Y. Kim, S. Mauro, N. Gevry, J. T. Lis, W. L. Kraus, *Cell* **119**, 803 (2004).
7. B. G. Ju *et al.*, *Cell* **119**, 815 (2004).
8. M. Malanga, F. R. Althaus, *Biochem. Cell Biol.* **83**, 354 (2005).
9. S. Burma, D. J. Chen, *DNA Repair* **3**, 909 (2004).
10. J. M. Jeltsch *et al.*, *Nucleic Acids Res.* **15**, 1401 (1987).
11. J. C. Wang, *Nat. Rev. Mol. Cell Biol.* **3**, 430 (2002).
12. A. Dvir, S. R. Peterson, M. W. Knuth, H. Lu, W. S. Dynan, *Proc. Natl. Acad. Sci. U.S.A.* **89**, 11920 (1992).
13. T. Chibazakura *et al.*, *Eur. J. Biochem.* **247**, 1166 (1997).
14. C. A. Sartorius, G. S. Takimoto, J. K. Richer, L. Tung, K. B. Horwitz, *J. Mol. Endocrinol.* **24**, 165 (2000).
15. G. L. Mayeur *et al.*, *J. Biol. Chem.* **280**, 10827 (2005).
16. C. Leontiou, J. H. Lakey, R. Lightowlers, R. M. Turnbull, C. A. Austin, *Mol. Pharmacol.* **69**, 130 (2006).
17. R. Metivier *et al.*, *Cell* **115**, 751 (2003).
18. L. Ko, G. R. Cardona, W. W. Chin, *Proc. Natl. Acad. Sci. U.S.A.* **97**, 6212 (2000).
19. S. K. Lee *et al.*, *Mol. Endocrinol.* **14**, 915 (2000).
20. J. Torchia *et al.*, *Nature* **387**, 677 (1997).
21. M. Binaschi, R. Farinosi, M. E. Borgnetto, G. Capranico, *Cancer Res.* **60**, 3770 (2000).
22. M. N. Cervellera, A. Sala, *J. Biol. Chem.* **275**, 10692 (2000).
23. P. O. Hassa, M. Covic, S. Hasan, R. Imhof, M. O. Hottiger, *J. Biol. Chem.* **276**, 45588 (2001).
24. C. Le Page, J. Sanceau, J. C. Drapier, J. Wietzerbin, *Biochem. Biophys. Res. Commun.* **243**, 451 (1998).
25. A. J. Butler, C. P. Ordahl, *Mol. Cell. Biol.* **19**, 296 (1999).
26. M. Ku, S. Stewart, A. Hata, *Biochem. Biophys. Res. Commun.* **311**, 702 (2003).
27. F. R. Althaus *et al.*, *Mol. Cell. Biochem.* **138**, 53 (1994).
28. D. T. Brown, *Biochem. Cell Biol.* **81**, 221 (2003).
29. J. O. Thomas, *Biochem. Soc. Trans.* **29**, 395 (2001).
30. M. F. Ruh, J. C. Chrivia, L. K. Cox, T. S. Ruh, *Mol. Cell. Endocrinol.* **214**, 71 (2004).
31. D. Das, R. C. Peterson, W. M. Scovell, *Mol. Endocrinol.* **18**, 2616 (2004).
32. A. M. Nunez, M. Berry, J. L. Imler, P. Chambon, *EMBO J.* **8**, 823 (1989).
33. T. Barkhem, L. A. Haldosen, J. A. Gustafsson, S. Nilsson, *Mol. Pharmacol.* **61**, 1273 (2002).
34. I. Collins, A. Weber, D. Levens, *Mol. Cell. Biol.* **21**, 8437 (2001).

35. We thank C. Nelson and K. Ohgi for their assistance; S. Ogawa and J. Puc for reagents; and X. Zhu and T. Wang for discussions and advice. We also thank J. Hightower and M. Fisher for assistance in figure and manuscript preparation and M. Gonzalez (Santa Cruz Biotechnology) for advice on reagents. M.G.R. is an investigator with the Howard Hughes Medical Institute and B.J. is supported by the U.S. Army Medical Research and Materiel Command (grant DAMD17-01-1-0184). These studies are supported by NIH and National Cancer Institute grants to M.G.R. and C.K.G.

Supporting Online Material

www.sciencemag.org/cgi/content/full/312/5781/1798/DC1
Materials and Methods
Figs. S1 to S5
References

9 March 2006; accepted 4 May 2006
10.1126/science.1127196

The Muscle Protein Dok-7 Is Essential for Neuromuscular Synaptogenesis

Kumiko Okada,[1]* Akane Inoue,[1]* Momoko Okada,[1] Yoji Murata,[1] Shigeru Kakuta,[3] Takafumi Jigami,[4] Sachiko Kubo,[3] Hirokazu Shiraishi,[5] Katsumi Eguchi,[5] Masakatsu Motomura,[5] Tetsu Akiyama,[4] Yoichiro Iwakura,[3] Osamu Higuchi,[1]† Yuji Yamanashi[1,2]†

The formation of the neuromuscular synapse requires muscle-specific receptor kinase (MuSK) to orchestrate postsynaptic differentiation, including the clustering of receptors for the neurotransmitter acetylcholine. Upon innervation, neural agrin activates MuSK to establish the postsynaptic apparatus, although agrin-independent formation of neuromuscular synapses can also occur experimentally in the absence of neurotransmission. Dok-7, a MuSK-interacting cytoplasmic protein, is essential for MuSK activation in cultured myotubes; in particular, the Dok-7 phosphotyrosine-binding domain and its target in MuSK are indispensable. Mice lacking Dok-7 formed neither acetylcholine receptor clusters nor neuromuscular synapses. Thus, Dok-7 is essential for neuromuscular synaptogenesis through its interaction with MuSK.

Skeletal muscle is controlled by motor neurons, which contact the muscle at the neuromuscular junction, a synapse that uses the neurotransmitter acetylcholine (*1*, *2*). To achieve sufficient sensitivity to the neurotransmitter, acetylcholine receptors (AChRs) on the muscle must be densely clustered on the postsynaptic side of the neuromuscular junction (*1*, *2*). Failure of AChR clustering is associated with disorders in neuromuscular transmission, including congenital myasthenic syndrome and myasthenia gravis (*3*, *4*). The presynaptic motor-nerve terminal secretes the glycoprotein agrin to activate postsynaptic MuSK (*5*). This agrin-dependent activation of MuSK is essential to establish the postsynaptic apparatus, including the clustering of AChRs, via the AChR-associated protein Rapsyn (*6*–*8*). Nevertheless, before innervation, MuSK-dependent AChR clusters can form at the endplate area of myotubes, suggesting a mechanism of postsynaptic specialization that is independent of agrin and innervation (*9*–*11*). Furthermore, neuromuscular synapses can form independently of agrin in mice that lack acetylcholine, which appears to antagonize postsynaptic differentiation (*12*, *13*). Thus, in addition to agrin, there may be another element that can achieve MuSK activation and trigger postsynaptic specializations at the neuromuscular junction. MuSK contains a phosphotyrosine-binding domain (PTB domain) target motif Asn-Pro-X-Tyr encompassing Tyr^{553} in the juxtamembrane region, which is essential for proper functioning in vivo (*14*). The binding partner for this motif has remained elusive.

By searching databases, including GenBank, the European Molecular Biology Laboratory, and the DNA Data Bank of Japan, for a previously unidentified member of the Dok-family of proteins, each of which has a PTB domain, we identified Dok-7 and cloned human cDNA encoding 504 amino acids. Like other members, Dok-7 has pleckstrin-homology (PH) and PTB domains in the N-terminal portion and Src homology 2 (SH2) domain target motifs in the C-terminal region (fig. S1) (*15*–*17*). Cloning of mouse (*Mus musculus*) and puffer fish (*Takifugu rubripes*) Dok-7 cDNA revealed a highly conserved structure (fig. S2). Like agrin and MuSK, no ortholog was found in invertebrates such as the fruit fly (*Drosophila melanogaster*) and nematode (*Caenorhabditis elegans*). Northern blot analysis of human tissues showed that Dok-7 mRNA is preferentially expressed in skeletal muscle and in the heart (fig. S3A), and immunoblot analysis identified a 55-kD Dok-7 protein in the thigh muscle, diaphragm, and heart but not in the liver or spleen (fig. S3B). Furthermore, immunostaining of mouse skeletal muscles, including the sternocleidomas-

[1]Department of Cell Regulation, Medical Research Institute, [2]School of Biomedical Science, Tokyo Medical and Dental University, Tokyo 113–8510, Japan. [3]Center for Experimental Medicine, Institute of Medical Science, University of Tokyo, Tokyo 108–8639, Japan. [4]Laboratory of Molecular and Genetic Information, Institute of Molecular and Cellular Biosciences, University of Tokyo, Tokyo 113–0032, Japan. [5]The First Department of Internal Medicine, Graduate School of Biomedical Sciences, Nagasaki University, Nagasaki 852–8501, Japan.

*These authors contributed equally to this work.
†To whom correspondence should be addressed. E-mail: yamanashi.creg@mri.tmd.ac.jp (Y.Y.); higuchi.creg@mri.tmd.ac.jp (O.H.)

toid, extensor digitorum longus, and gastrocnemius, with antiserum to Dok-7 highlighted the accumulation of Dok-7 at neuromuscular junctions (Fig. 1, A to C), which are composed of the postsynaptic membrane with its densely clustered AChRs in close juxtaposition with the presynaptic nerve terminal. Therefore, we denervated a mouse gastrocnemius muscle by sciatic nerve resection to confirm the muscular, and thus postsynaptic, localization of Dok-7. One week after the operation, synaptophysin, a component of the presynaptic vesicle, was completely abolished in denervated muscles (fig. S4). However, the muscular localization of Dok-7 and AChRs remained intact, indicating a postsynaptic localization of Dok-7 at neuromuscular junctions (Fig. 1, D to F). Because postsynaptic differentiation and neuromuscular synapse formation are initiated at the endplate zone of skeletal muscle during embryogenesis (*9*–*11*), we performed a whole-mount in situ hybridization and found that Dok-7 transcripts are expressed in the central region encompassing the endplate area of the diaphragm muscles at day 14.5 of embryonic development (E14.5), when AChRs cluster in a nerve- and agrin-independent manner (fig. S5). Together, these results suggest that Dok-7 has the appropriate distribution to be involved in the neuromuscular junction.

Given the requirement for MuSK's PTB target motif and presumably its binding partner in postsynaptic specialization (*14*, *18*, *19*), we next examined the interaction of MuSK with Dok-7, which has a PTB domain, in 293T cells. These heterologous cells do not express either protein detectably, and forced expression of MuSK in these cells induced weak

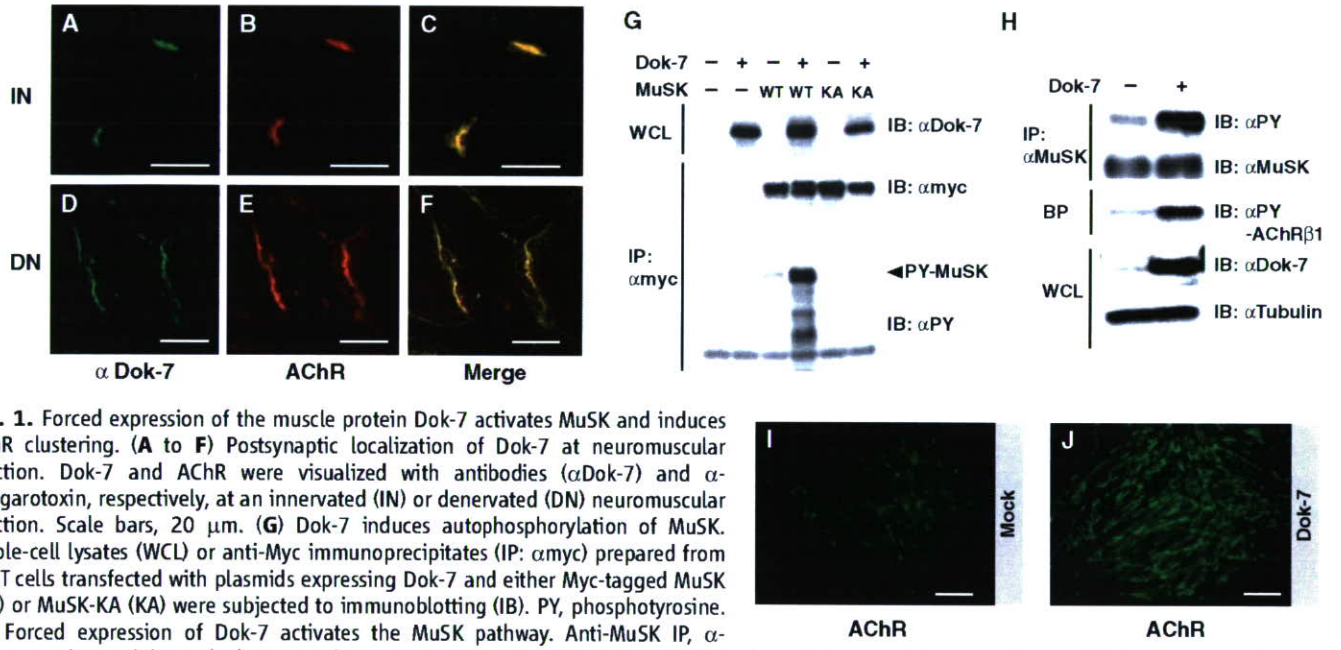

Fig. 1. Forced expression of the muscle protein Dok-7 activates MuSK and induces AChR clustering. (**A** to **F**) Postsynaptic localization of Dok-7 at neuromuscular junction. Dok-7 and AChR were visualized with antibodies (αDok-7) and α-bungarotoxin, respectively, at an innervated (IN) or denervated (DN) neuromuscular junction. Scale bars, 20 μm. (**G**) Dok-7 induces autophosphorylation of MuSK. Whole-cell lysates (WCL) or anti-Myc immunoprecipitates (IP: αmyc) prepared from 293T cells transfected with plasmids expressing Dok-7 and either Myc-tagged MuSK (WT) or MuSK-KA (KA) were subjected to immunoblotting (IB). PY, phosphotyrosine. (**H**) Forced expression of Dok-7 activates the MuSK pathway. Anti-MuSK IP, α-bungarotoxin precipitates (BP), or WCL from C2 myotubes transfected with plasmids for Dok-7 were subjected to IB. (**I** and **J**) Forced expression of Dok-7 induces aneural AChR clustering in C2 myotubes. Abundant clusters of AChRs formed in C2 myotubes transfected with Dok-7 expression plasmids (J), but only a few small clusters formed in the control (Mock) (I). Scale bars, 200 μm.

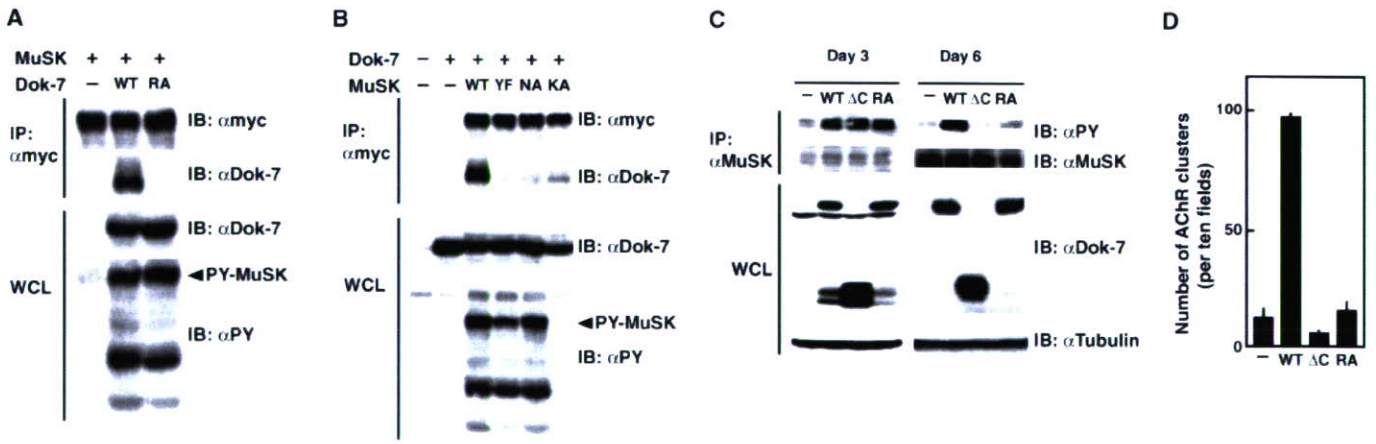

Fig. 2. Dok-7 interacts with MuSK by way of the PTB domain. (**A** and **B**) The PTB domain, its target, and kinase activity are essential for Dok-7 binding to MuSK. Anti-Myc IP or WCL from 293T cells transfected with plasmids for Dok-7 and Myc-tagged MuSK or their mutants, including MuSK-KA, were subjected to IB. (**C** and **D**) The PTB domain and C-terminal region are indispensable for the Dok-7–induced activation of MuSK and AChR clustering in fully differentiated C2 myotubes. Anti-MuSK IP or WCL from C2 cells transfected with expression plasmids for Dok-7 (WT), Dok-7–ΔC (ΔC), or Dok-7–RA (RA) were prepared at day 3 or 6 upon differentiation into myotubes and subjected to IB (C). The number of AChR clusters (mean ± SD) counted at day 7 is shown (D). Differentiation was achieved by day 6, whereas only a few myotubes had formed by day 3.

autophosphorylation (*20*, *21*). Forced expression of Dok-7 induced an intense tyrosine phosphorylation of MuSK but not the kinase-inactive mutant with a Lys/Ala substitution (MuSK-KA), indicating that Dok-7 induced the autophosphorylation of MuSK (Fig. 1G). This activity was unique to Dok-7; no other mammalian Dok-family proteins induced phosphorylation of MuSK (fig. S6). It was also conserved; Dok-7 from puffer fish was able to activate even mammalian MuSK. Also, in C2 myotubes, the forced expression of Dok-7 induced tyrosine phosphorylation of MuSK and the β subunit (AChRβ1) of the AChR complex, which is known to be tyrosine-phosphorylated upon activation of MuSK (*22*) (Fig. 1H). Furthermore, this forced expression induced numerous clusters of AChRs, and the number of AChR clusters correlated with the amount of Dok-7 expression plasmid (Fig. 1, I and J; fig. S7A and supporting online material). The exogenous Dok-7–induced AChR clusters were elaborately branched, and their complicated architecture resembled the differentiated "pretzel-like" AChR clusters formed in vivo (fig. S7, B and C). In addition, forced expression in myotubes of Dok-7 that had been fused with enhanced green fluorescent protein (EGFP) induced Dok-7 and AChR coclustering (fig. S7, D to I), as observed at postsynaptic areas in vivo (Fig. 1, C and F).

Because the regulatory interaction of Dok-7 with MuSK as described above implies their physical interaction, we examined whether Dok-7 binds to MuSK by way of the PTB domain in 293T cells. MuSK was coimmunoprecipitated with Dok-7 but not with Dok-7 carrying three Arg/Ala substitutions (Dok-7–RA) in the PTB domain (Fig. 2A). Consistently, the mutant MuSK carrying either a Tyr/Phe substitution at Tyr^{553} (MuSK-YF) or an Asn/Ala substitution at Asn^{550} (MuSK-NA) in the PTB target motif was not coimmunoprecipitated with Dok-7 (fig. S9 and Fig. 2B). The failure of the MuSK-KA kinase-inactive mutant to be coimmunoprecipitated with Dok-7 confirms the requirement of tyrosine phosphorylation for the binding of MuSK with Dok-7 via the PTB domain. These results indicate that Dok-7 binds to MuSK through the PTB domain in a manner dependent on the tyrosine phosphorylation of its target motif in MuSK.

Nevertheless, mutations in the PTB domain (Dok-7–RA) or PTB target motif (MuSK-NA or -YF) did not block activation of MuSK, at least in heterologous cells (Fig. 2, A and B). In addition, the N- and C-terminal deletion mutants of Dok-7 (Dok-7-ΔN and -ΔC) revealed that the C-terminal moiety, but not the PH domain, of Dok-7 is dispensable for MuSK activation in heterologous cells (fig. S10). Also, the forced expression of Dok-7–RA or Dok-7–ΔC induced MuSK activation even in C2 cells at day 3 of differentiation into myotubes (Fig. 2C), when very few myotubes have formed. Unexpectedly, however, the PTB domain and C-terminal portion were indispensable for Dok-7–induced MuSK activation and AChR clustering in fully differentiated C2 myotubes at days 6 and 7 of differentiation (Fig. 2, C and D). In addition, the PH domain, responsible for membrane localization in general, was indispensable for the activation of MuSK in fully differentiated myotubes (fig. S11), as was seen in heterologous cells (fig. S10). Together these findings suggest that a negative regulatory mechanism preventing MuSK activation is established upon differentiation into myotubes, which is accompanied by increased expression of MuSK and Dok-7 (fig. S12). Trace phosphorylation of MuSK in myotubes might allow physical interaction with Dok-7, in turn facilitating dimerization and/or conformational changes in MuSK that are necessary for its sustained activation.

MuSK-deficient myotubes do not form agrin-dependent or -independent clusters of AChRs unless MuSK is reintroduced (*18*, *19*, *23*). To confirm whether Dok-7–mediated AChR clustering is dependent on MuSK, we introduced Dok-7 into MuSK-deficient myotubes. Unlike its effect in C2 myotubes, forced expression of Dok-7 induced no AChR clustering in the MuSK-deficient myotubes; however, additional expression of wild-type MuSK resulted in robust clustering of AChRs in these cells (Fig. 3A). Furthermore, the MuSK-KA and MuSK-YF mutant each failed to complement the MuSK deficiency, regardless of exogenous Dok-7. These findings demonstrate that Dok-7–induced AChR clustering in myotubes depends on Dok-7 interaction with MuSK and subsequent activation of MuSK catalytic activity. Thus, we examined the regulatory interaction of Dok-7 with a MuSK mutant [MuSK-Val/Met (MuSK-VM)] that carries a Val^{790} to Met substitution. This mutation is causally associated with the congenital myasthenic syndrome by way of an as yet unclear mechanism (*24*). As observed with MuSK-YF (Fig. 2B), forced expression of Dok-7 in 293T cells induced the autophosphorylation of MuSK-VM, but its coimmunoprecipitation with Dok-7 was barely detectable in these heterologous cells (fig. S13). Forced expression of Dok-7 with MuSK-VM induced only very weak AChR clustering in MuSK-deficient myotubes (Fig. 3A). Therefore, the congenital myasthenic syndrome–associated Val^{790} to Met mutation impaired interaction of MuSK with Dok-7, suggesting a possible cause of neuromuscular junction dysfunction in these patients.

To examine the effects of Dok-7 down-regulation in myotubes, we used a small interfering RNA (siRNA) designed specifically to block its expression. Inhibition of Dok-7 suppressed the tyrosine phosphorylation of

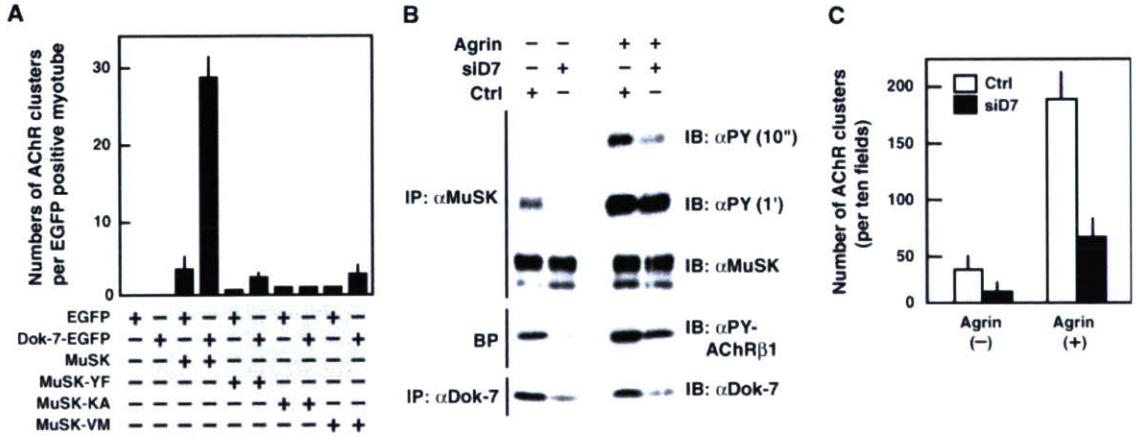

Fig. 3. Dok-7 is essential for activation of the MuSK-pathway to AChR clustering in myotubes. **(A)** MuSK is required for Dok-7–induced AChR clustering. MuSK-deficient myotubes were transfected with the indicated plasmids. The number of AChR clusters (mean ± SD) per EGFP-positive myotube is shown. MuSK-VM is a congenital myasthenic syndrome–associated mutant. **(B)** Activation of the MuSK pathway requires Dok-7. C2 myotubes transfected with Dok-7 siRNA (siD7) or the control (Ctrl) without (−) or with (+) agrin treatment for 15 min were studied as in Fig. 1H. Both short [10 s (10″)] and long [1 min (1′)] exposures are shown for the anti-PY IB of the anti-MuSK IP. **(C)** Dok-7 is essential for AChR clustering. C2 myotubes were transfected with Dok-7 siRNA (siD7) or the control (Ctrl) with or without agrin treatment for 12 hours. The number of AChR clusters (mean ± SD) is shown.

MuSK and AChRβ1 in C2 myotubes, demonstrating its essential role in the aneural, basal catalytic activity of MuSK (Fig. 3B). Indeed, MuSK-dependent spontaneous AChR clustering was suppressed by this siRNA-mediated inhibition (Fig. 3C). Moreover, the inhibition of Dok-7 impaired the agrin-dependent activation of MuSK, the phosphorylation of AChRβ1, and the subsequent formation of AChR clusters (Fig. 3, B and C). Thus, we conclude that Dok-7 is essential for aneural activation of MuSK and AChR clustering in myotubes and is also crucial for agrin-dependent activation of MuSK and AChR clustering. Nonetheless, our results do not exclude the possibility that Dok-7 might also play a role downstream of MuSK. Indeed, Dok-7 and MuSK were synchronously tyrosine phosphorylated upon treatment of myotubes with agrin (fig. S14).

We generated mice lacking Dok-7 to explore its role in vivo (fig. S15). Like mice lacking MuSK or agrin (*6*, *7*), all Dok-7–deficient (Dok-7$^{-/-}$) mice were immobile at birth and died shortly thereafter (26 homozygotes were observed among the first 137 pups), although their wild-type and heterozygous littermates appeared normal. Also, the alveoli of the mutant mice were not expanded at birth (fig. S15D), indicating a failure to breathe and suggesting a severe defect in neuromuscular transmission in the skeletal muscles. Consistently, there were no detectable AChR clusters in the endplate area of the diaphragm muscle in Dok-7$^{-/-}$ embryos at either E14.5 or E18.5 (Fig. 4, E and K). Because nascent AChR clusters are formed in a nerve- and agrin-independent manner at E13.5 to E16.5, whereas most neuromuscular junctions are formed in a nerve- and agrin-dependent manner at E18.5, our findings indicate a requirement for Dok-7 in both types of MuSK-dependent postsynaptic specialization, although we cannot exclude the possibility that nascent AChR clustering is a prerequisite for nerve- and agrin-dependent AChR clustering (*9*–*11*). Consistent with this finding, Dok-7 transcripts were expressed in the endplate area of the diaphragm muscle (fig. S5). In addition, axonal branches extending from the motor nerve trunk were aberrantly long in the endplate area of Dok-7$^{-/-}$ diaphragms at E18.5 and, unlike the controls, did not terminate near the nerve trunk (Fig. 4, G and J). Overall, these pre- and postsynaptic abnormalities are indistinguishable from those found in mice lacking MuSK (*7*), demonstrating an essential role in vivo for Dok-7 in neuromuscular synaptogenesis, a MuSK-dependent vital process.

MuSK-dependent postsynaptic specialization during neuromuscular synaptogenesis appears to be controlled by multiple regulatory mechanisms (*2*, *25*). We have shown that Dok-7 may be a muscle-intrinsic activator of MuSK by demonstrating its essential role in the aneural activation of MuSK and subsequent AChR clustering in cultured myotubes. This conclusion is further supported by our findings that mice lacking Dok-7 showed marked disruption of neuromuscular synaptogenesis that was indistinguishable from the disruption found in MuSK-deficient mice. Thus, neuromuscular synaptogenesis requires Dok-7 within the skeletal muscle. Dok-7 dysfunction may be involved in the pathogenesis of neuromuscular junction disorders.

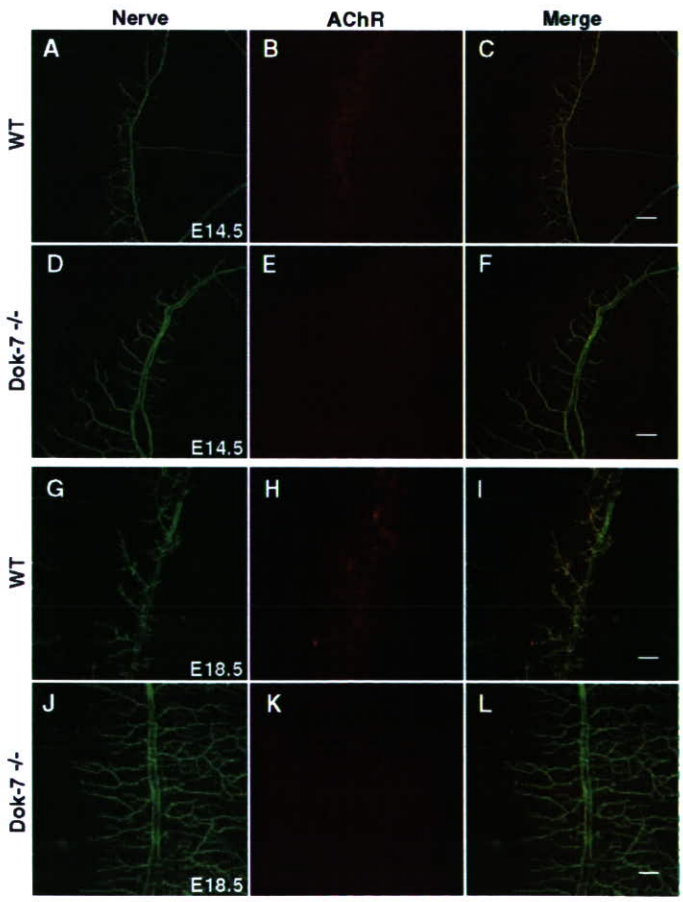

Fig. 4. Dok-7 is essential for neuromuscular synaptogenesis in vivo. Diaphragm muscles were prepared from the wild-type control (WT) or Dok-7$^{-/-}$ embryos at E14.5 (**A** to **F**) or E18.5 (**G** to **L**) and subjected to whole-mount anti-neurofilament and α-bungarotoxin staining, to visualize nerve and AChR, respectively. Scale bars, 100 μm.

References and Notes

1. S. J. Burden, *Genes Dev.* **12**, 133 (1998).
2. J. R. Sanes, J. W. Lichtman, *Nat. Rev. Neurosci.* **2**, 791 (2001).
3. A. G. Engel, K. Ohno, S. M. Sine, *Nat. Rev. Neurosci.* **4**, 339 (2003).
4. A. Vincent *et al.*, *Ann. N. Y. Acad. Sci.* **998**, 324 (2003).
5. D. J. Glass *et al.*, *Cell* **85**, 513 (1996).
6. M. Gautam *et al.*, *Cell* **85**, 525 (1996).
7. T. M. DeChiara *et al.*, *Cell* **85**, 501 (1996).
8. M. Gautam *et al.*, *Nature* **377**, 232 (1995).
9. W. Lin *et al.*, *Nature* **410**, 1057 (2001).
10. X. Yang *et al.*, *Neuron* **30**, 399 (2001).
11. X. Yang, W. Li, E. D. Prescott, S. J. Burden, J. C. Wang, *Science* **287**, 131 (2000).
12. T. Misgeld, T. T. Kummer, J. W. Lichtman, J. R. Sanes, *Proc. Natl. Acad. Sci. U.S.A.* **102**, 11088 (2005).
13. W. Lin *et al.*, *Neuron* **46**, 569 (2005).
14. R. Herbst, E. Avetisova, S. J. Burden, *Development* **129**, 5449 (2002).
15. N. Carpino *et al.*, *Cell* **88**, 197 (1997).
16. Y. Yamanashi, D. Baltimore, *Cell* **88**, 205 (1997).
17. R. J. Crowder, H. Enomoto, M. Yang, E. M. Johnson Jr., J. Milbrandt, *J. Biol. Chem.* **279**, 42072 (2004).
18. H. Zhou, D. J. Glass, G. D. Yancopoulos, J. R. Sanes, *J. Cell Biol.* **146**, 1133 (1999).
19. R. Herbst, S. J. Burden, *EMBO J.* **19**, 67 (2000).
20. A. Watty *et al.*, *Proc. Natl. Acad. Sci. U.S.A.* **97**, 4585 (2000).
21. S. K. H. Gillespie, S. Balasubramanian, E. T. Fung, R. L. Huganir, *Neuron* **16**, 953 (1996).
22. C. Fuhrer, J. E. Sugiyama, R. G. Taylor, Z. W. Hall, *EMBO J.* **16**, 4951 (1997).
23. J. E. Sugiyama, D. J. Glass, G. D. Yancopoulos, Z. W. Hall, *J. Cell Biol.* **139**, 181 (1997).
24. F. Chevessier *et al.*, *Hum. Mol. Genet.* **13**, 3229 (2004).
25. T. T. Kummer, T. Misgeld, J. R. Sanes, *Curr. Opin. Neurobiol.* **16**, 74 (2006).

26. We thank Regeneron Pharmaceuticals for MuSK-deficient cells; K. Manji, J. Hamuro, H. Moriya, and A. Ishii for technical assistance; and M. Shirakata, T. Yasuda, S. Sugano, T. Tezuka, R. F. Whittier, S. Tronick, and T. Yamamoto for discussions. This work was supported by Grants-in-Aid for Scientific Research from the Ministry of Education, Culture, Sports, Science and Technology and by a grant from the Uehara Foundation.

Supporting Online Material

www.sciencemag.org/cgi/content/full/312/5781/1802/DC1
Materials and Methods
SOM Text
Figs. S1 to S15
References

8 March 2006; accepted 19 May 2006
10.1126/science.1127142

Available online at www.sciencedirect.com
SCIENCE DIRECT
ELSEVIER
Biochemical and Biophysical Research Communications 343 (2006) 719–730
BBRC
www.elsevier.com/locate/ybbrc

Alteration of familial ALS-linked mutant SOD1 solubility with disease progression: Its modulation by the proteasome and Hsp70

Shingo Koyama [a], Shigeki Arawaka [a,*], Ren Chang-Hong [a], Manabu Wada [a], Toru Kawanami [a], Keiji Kurita [a], Masaaki Kato [b], Makiko Nagai [b], Masashi Aoki [b], Yasuto Itoyama [b], Gen Sobue [c], Pak H. Chan [d], Takeo Kato [a]

[a] *Department of Neurology, Hematology, Metabolism, Endocrinology and Diabetology, Yamagata University School of Medicine, 2-2-2 Iida-nishi, Yamagata 990-9585, Japan*
[b] *Department of Neurology, Tohoku University Graduate School of Medicine, Sendai, Japan*
[c] *Department of Neurology, Nagoya University Graduate School of Medicine, Nagoya, Japan*
[d] *Department of Neurosurgery, Stanford University School of Medicine, Stanford, CA, USA*

Received 9 February 2006
Available online 9 March 2006

Abstract

Accumulation of misfolded Cu/Zn superoxide dismutase (SOD1) occurs in patients with a subgroup of familial amyotrophic lateral sclerosis (fALS). To identify the conversion of SOD1 from a normally soluble form to insoluble aggregates, we investigated the change of SOD1 solubility with aging in fALS-linked H46R SOD1 transgenic mice. Mutant SOD1 specifically altered to insoluble forms, which were sequentially separated into Triton X-100-insoluble/sodium dodecyl sulfate (SDS)-soluble and SDS-insoluble/formic acid-soluble species. In spinal cords, the levels of SDS-dissociable soluble SOD1 monomers and SDS-stable soluble dimers were significantly elevated before motor dysfunction onset. In COS-7 cells expressing H46R SOD1, treatment with proteasome inhibitors recapitulated the alteration of SOD1 solubility in transgenic mice. In contrast, overexpression of Hsp70 reduced accumulation of mutant-specific insoluble SOD1. SDS-soluble low molecular weight species of H46R SOD1 may appear as early misfolded intermediates when their concentration exceeds the capacity of the proteasome and molecular chaperones.

Keywords: Amyotrophic lateral sclerosis; Cu/Zn superoxide dismutase; Heat shock protein; Proteasome; Oligomer

Amyotrophic lateral sclerosis (ALS) is a neurodegenerative disorder characterized by the degeneration of both upper and lower motor neurons, leading to progressive paralysis. Of all ALS cases, ~90% are sporadic and ~10% are familial; ~20% of familial ALS (fALS) cases are associated with dominantly inherited mutations in the gene encoding Cu/Zn superoxide dismutase (SOD1) [1–3]. SOD1 is a major antioxidant enzyme located predominantly in the cytosol, nucleus, and mitochondrial intermembrane space of eukaryotic cells [4]. The biological active enzyme forms a 32-kDa homodimer and contains one copper-binding site and one zinc-binding site, as well as a disulfide bond in each of its two subunits. SOD1-linked fALS was initially suspected to result from oxidative damage caused by diminished SOD1 activity, but SOD1-null mice show no motor neuron disease [5], and transgenic mice overexpressing human mutant SOD1 have a phenotype that is closely similar to patients with fALS, irrespective of their normal or elevated levels of SOD1 activity [6–9]. This evidence indicates that SOD1-linked fALS occurs due to a toxic gain-of-function of mutant SOD1 but not due to a lowering of its activity [6].

Deposition of proteinaceous inclusions of SOD1 in motor neurons is a characteristic hallmark of patients with fALS [10–12]. Cellular and animal models have shown that overexpression of mutant SOD1 can cause loss of motor

* Corresponding author. Fax: +81 23 628 5318.
E-mail address: arawaka@med.id.yamagata-u.ac.jp (S. Arawaka).

0006-291X/$ - see front matter © 2006 Elsevier Inc. All rights reserved.
doi:10.1016/j.bbrc.2006.02.170